ChemSusChem

Review
doi.org/10.1002/cssc.202402018

Chemistry Europe
European Chemical Societies Publishing

www.chemsuschem.org

Unveiling the Potential of Heterogeneous Systems for Reversible Hydrogen Storage in Liquid Organic Hydrogen Carriers

Jyothi Jangir[a] and Balaji R. Jagirdar*[a]

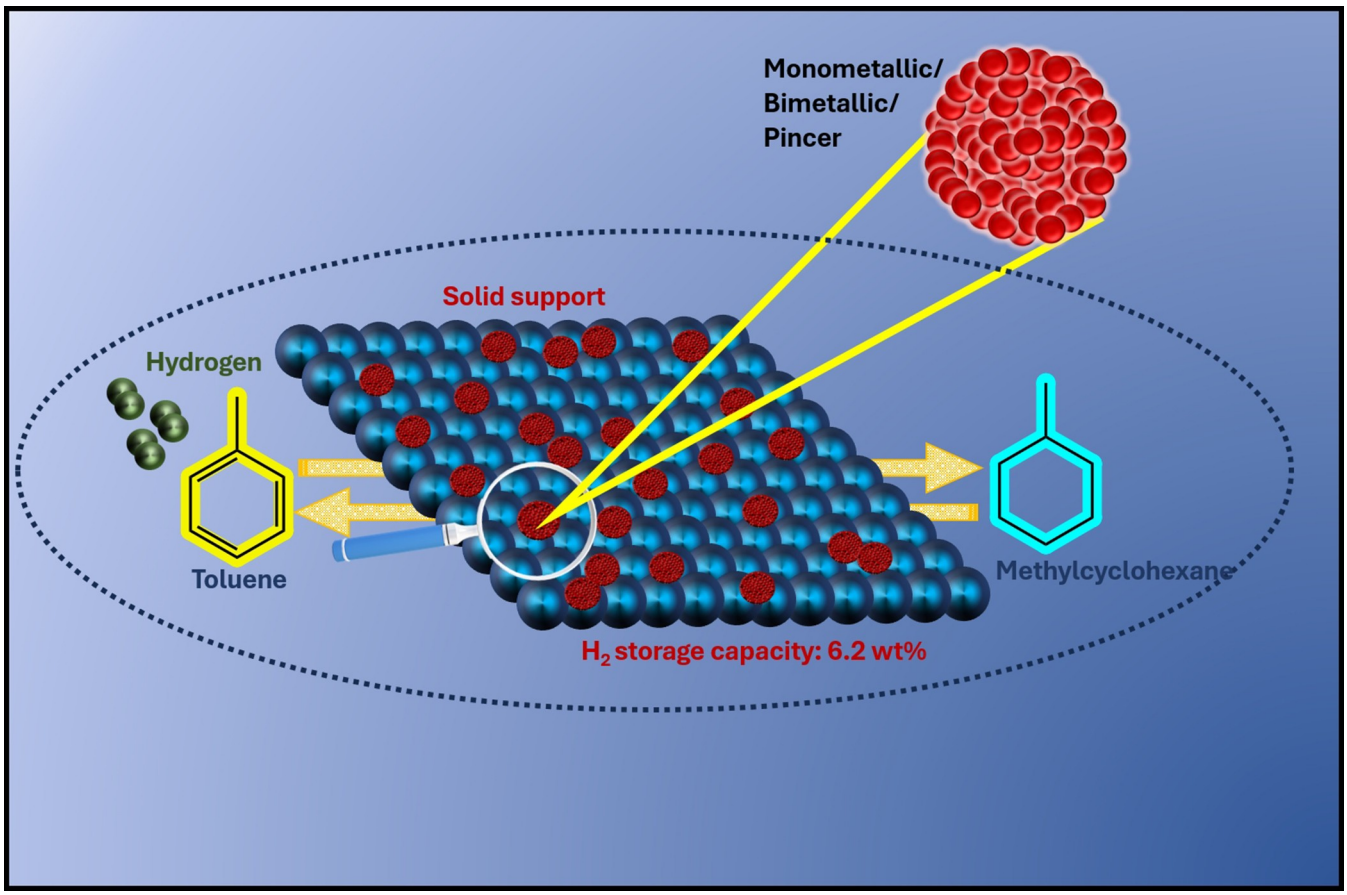

Transitioning towards a carbon-free economy is the current global need of the hour. The transportation sector is one of the major contributors of CO_2 emissions in the atmosphere disturbing the delicate balance on the Earth, leading to global warming. Hydrogen has emerged as a promising alternative energy carrier capable of replacing fossil fuels, with advancements in systems facilitating its storage and long-distance transport. In this context, the concept of liquid organic hydrogen carriers (LOHCs) is taking the lead, offering a plausible solution because of its compatibility with the existing gasoline infrastructure, while eliminating the challenges associated with the conventional hydrogen storage methods. Key LOHC systems, such as methylcyclohexane/toluene and H-18-dibenzyltoluene/dibenzyltoluene (H-18-DBT/DBT), have been extensively researched for large-scale applications. However, challenges persist, particularly concerning the endothermic nature of the reactions involved. In this regard, of particular interest are the multifunctional heterogeneous catalysts supported on a single support, offering cost-effective and energy-efficient solutions to circumvent issues related to the endothermicity of the reactions. In this review, solid heterogeneous catalysts that have been developed and investigated for reversible dehydrogenation and hydrogenation reactions have been presented. These catalysts include monometallic, bimetallic, and pincer complexes supported on materials designed for efficient hydrogen uptake and release.

1. Introduction

The COVID-19 pandemic initially led to a significant 5.1% decrease in global CO_2 emissions, showcasing the potential impact of reduced human activity on greenhouse gas emissions. However, this decline was short-lived as emissions rebounded, surpassing the 2020 levels by over 2.0 Gt in 2021, marking the largest year-on-year increase in energy-related CO_2 emissions.[1] Annually, around 7×10^{12} kg of carbon is introduced into the atmosphere through fossil fuel consumption and deforestation, with the transportation sector being a major contributor.[2] One effective approach to reducing these emissions is by using hydrogen (H_2) as an alternative energy carrier due to its environmental friendliness and high energy capacity. While hydrogen offers significant advantages as an energy carrier, challenges in its storage, limit its widespread adoption. Its low volumetric energy density (0.01 MJ/L or 3 Wh/L) makes storage under ambient conditions difficult, despite its high gravimetric energy density (33.0 kWh/kg).[3] Achieving suitable storage forms of hydrogen is crucial for applications like automotive and portable electronics. Various materials have been investigated for hydrogen storage, each with its own set of compromises between gravimetric and volumetric energy density. In this context, liquid organic hydrogen carriers (LOHCs) represent a promising solution that achieves a balance between these two factors. The U.S. Department of Energy, considering parameters like energy density, cost, charging/discharging rates, reversibility, and environmental safety has set targets (5.5 wt% for 2025) for hydrogen storage materials.[4] Currently, the research is being focused on designing materials that meet these targets to enable efficient onboard storage and usage in light-duty fuel vehicles.

[a] *Department of Inorganic and Physical Chemistry, Indian Institute of Science, Bangalore, India*

Correspondence: *Balaji R. Jagirdar, Department of Inorganic and Physical Chemistry, Indian Institute of Science, Bangalore 560 012, India.*
Email: jagirdar@iisc.ac.in

1.1. Traditional Hydrogen Storage Techniques

Storing hydrogen in the form of liquid or compressed gas involves energy-intensive processes, and rigorous safety requirements due to the low temperature (21 K) and high pressures (700–800 bar).[5] Additionally, hydrogen can also be stored in the solid form, in chemical bonds in ammonia borane,[6] metallic hydrides[7] like MgH_2 (7.6 wt%), $LaNi_5H_6$ (1.37 wt%), and $NaAlH_4$, physical adsorption in porous materials,[8] and organic frameworks.[9] However, the practical application of solid-state hydrogen storage materials is limited due to the high energy required for hydrogen desorption and kinetic limitations. Consequently, liquid-based storage remains necessary for industries like transportation, and thus LOHCs have garnered much interest worldwide, as a potential hydrogen carrier for the transportation industry.

2. Liquid Organic Hydrogen Carriers: The Concept

LOHCs are a pair of organic compounds capable of effectively carrying and releasing hydrogen in their hydrogen-rich/lean forms.[10,11] In their saturated form, LOHCs transport hydrogen, which could be released through dehydrogenation at the required site, converting the compound back to its hydrogen-lean state (Figure 1). After hydrogen consumption, hydrogen is to be reloaded into the unsaturated system, to close the cycle. The LOHCs offer several key advantages, making them an appealing energy storage and transport option.[5,10,12] They are cost-effective, safe, and theoretically enable long-term energy storage without the risk of boil-off losses. One of the notable benefits of LOHCs is their ability to be transported over medium to long distances without self-discharging, facilitating seasonal energy storage and delivery to remote areas. The compounds are not consumed during the reversible dehydrogenation-hydrogenation processes, enhancing their sustainability. Moreover, the existing pipeline infrastructure can be utilized for distribution, further increasing the appeal of the LOHC technology.

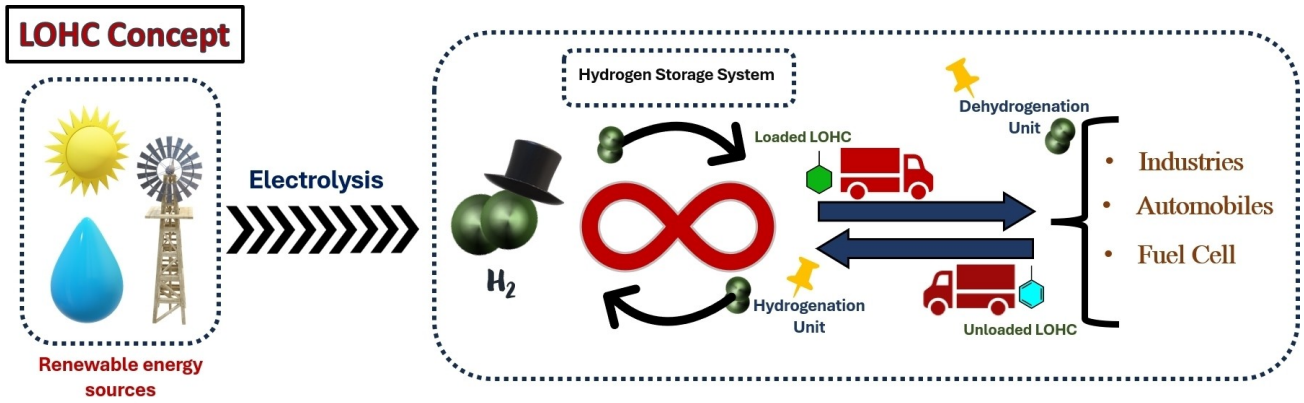

Figure 1. Schematic showing the concept of LOHCs.

When evaluating LOHCs, several important characteristics must be considered.[13] Beyond possessing a good hydrogen storage capacity, they should have a high boiling point to prevent volatilization and an efficient method for hydrogen separation during release. A low melting point (below 243 K) is also essential for effective hydrogen purification. The system should support multiple charging and discharging cycles throughout the hydrogenation and dehydrogenation processes. Additionally, to efficiently release hydrogen, the system must feature a low heat of desorption (between 42 and 54 kJ/mol H_2) and be available at a large scale and low cost.

Despite outlining the criteria for a viable LOHC system, it is evident that no existing LOHC fully meets all these conditions for practical applications. While LOHCs present promising opportunities for a sustainable energy future, significant limitations remain, necessitating further research and development before widespread global use.[20] One of the primary challenges is the high endothermic nature of the dehydrogenation reaction, which not only requires elevated temperatures but also leads to the formation of undesirable byproducts and coking. For example, in the cyclohexane/benzene system, the flammability of cyclohexane and the toxicity of benzene, along with the low boiling point of cyclohexane (354 K), complicate the release of high-quality hydrogen. The decalin/naphthalene system faces challenges, particularly due to naphthalene's high melting point and the irreversibility of the dehydrogenation reaction. Similarly, N-ethyl carbazole (NEC), with a melting point of 341 K, presents limitations. Carbazole-based derivatives encounter issues as well, as they decompose at high temperatures required for dehydrogenation, resulting in N-alkyl bond cleavage and dealkylation. For hydrocarbons like methylcyclohexane (MCH) and H-18 dibenzyl toluene (H-18 DBT), high dehydrogenation temperatures lead to catalyst deactivation, unwanted side product formation, and coking.[13]

Ultimately, a trade-off must be made between the endothermicity and the cost of LOHC systems, depending on their intended applications. While cyclic hydrocarbons like MCH and H-18 DBT require high temperatures for dehydrogenation,

Jyothi Jangir completed her M.Sc. degree from St Joseph's University, Bangalore, India. She is currently working with Prof. Balaji R. Jagirdar, as a Ph.D. scholar at the Indian Institute of Science, Bangalore, India. Her research interests include designing hybrid heterogeneous catalysts for tandem catalytic reactions and reversible hydrogen storage in Liquid Organic Hydrogen Carriers (LOHCs).

Balaji R. Jagirdar obtained his M.Sc. in chemistry from the Indian Institute of Technology (I.I.T.) Bombay, Mumbai, India in 1989, and his Ph.D. in chemistry from Kansas State University, Manhattan, Kansas, USA in 1994. He was a postdoctoral researcher at the University of Colorado, Boulder, Colorado, USA from 1994 to 1995 before returning to India in October 1995 to join the faculty of the Department of Inorganic and Physical Chemistry at the Indian Institute of Science, Bangalore, India. He joined as a lecturer and rose to the rank of a full professor in 2011. His research interests include the activation of small molecules using organometallic compounds, homogeneous and heterogeneous catalysis, nanostructured materials and their applications, and materials for hydrogen storage and generation.

heterocyclic hydrocarbons present an alternative, albeit at a higher initial raw material cost. Addressing these limitations is crucial for advancing LOHC technology toward practical implementation.[14]

2.1. Potential LOHC Systems

LOHCs are compounds with specific physical and chemical properties, which are crucial for hydrogen storage and transportation. Ideal LOHCs are those that have low melting points (< 243 K), high boiling points (> 573 K), good thermal stability, and low viscosity, particularly for automotive applications.[11] Reversible dehydrogenation and hydrogenation reactions, high gravimetric energy density (> 56 kg/m^3, > 6 wt%), and low heat of H_2 desorption (42–54 kJ/mol H_2) are essential criteria, with the US DOE setting a gravimetric and volumetric target of about 5.5 wt% and 40 g L^{-1} respectively, for LOHC compounds.[10,12–15] Environmental considerations, including low toxicity and eco-toxicological parameters, are important in LOHC selection. Detailed hazard assessments are necessary before widespread LOHC adoption, focusing on mutagenic and carcinogenic effects, as demonstrated by studies on heteroaromatic amines and carbazoles.[16,17] Chemical substitution can significantly influence mutagenic activity, highlighting the importance of considering chemical parameters and ecotoxicity in LOHC selection.

LOHC development started with the methylcyclohexane-toluene system by Knecht and colleagues,[18] followed by Pez et al.'s patent in 2006 on reversible hydrogenation in π-conjugated aromatic compounds.[19] Studies on LOHCs are typically focused on homocyclic alkanes, N-heterocycles and circular hydrogen carriers.[10,20–24] Among the homocyclic alkanes, cycloalkanes like cyclohexane,[25–28] methylcyclohexane,[27,29,30] dibenzyl toluene,[31–35] and decalin[36,37] have been extensively studied. Some of the most important LOHC systems that have been studied in the last decade are shown in Figure 2. Subsequent investigations in this field explored various other hydrocarbons. These compounds exhibit high hydrogen storage capacities of approximately 6–8 wt% and volumetric capacities of around 60–62 g/L, meeting the LOHC criteria along with high boiling points and storage properties. The methylcyclohexane/toluene (MCH/Tol) and H-18-dibenzyltoluene/dibenzyltoluene (H-18-DBT/DBT) are particularly preferred and widely studied LOHC systems due to their high hydrogen storage capacity. However, their notable limitations lie in the high enthalpy requirement (64–69 kJ/mol H_2) for dehydrogenation, often occurring at temperatures of 573 K–623 K. At such high temperatures, the systems are also prone to C–C bond cleavage and coking, leading to catalyst deactivation.[10] Another challenge with the H18-DBT system, is the process of dehydrogenation-hydrogenation which generates intermediates that result upon incomplete reactions, consequently reducing the hydrogen storage capacity. The drawback with these cyclic hydrocarbons is also the carcino-

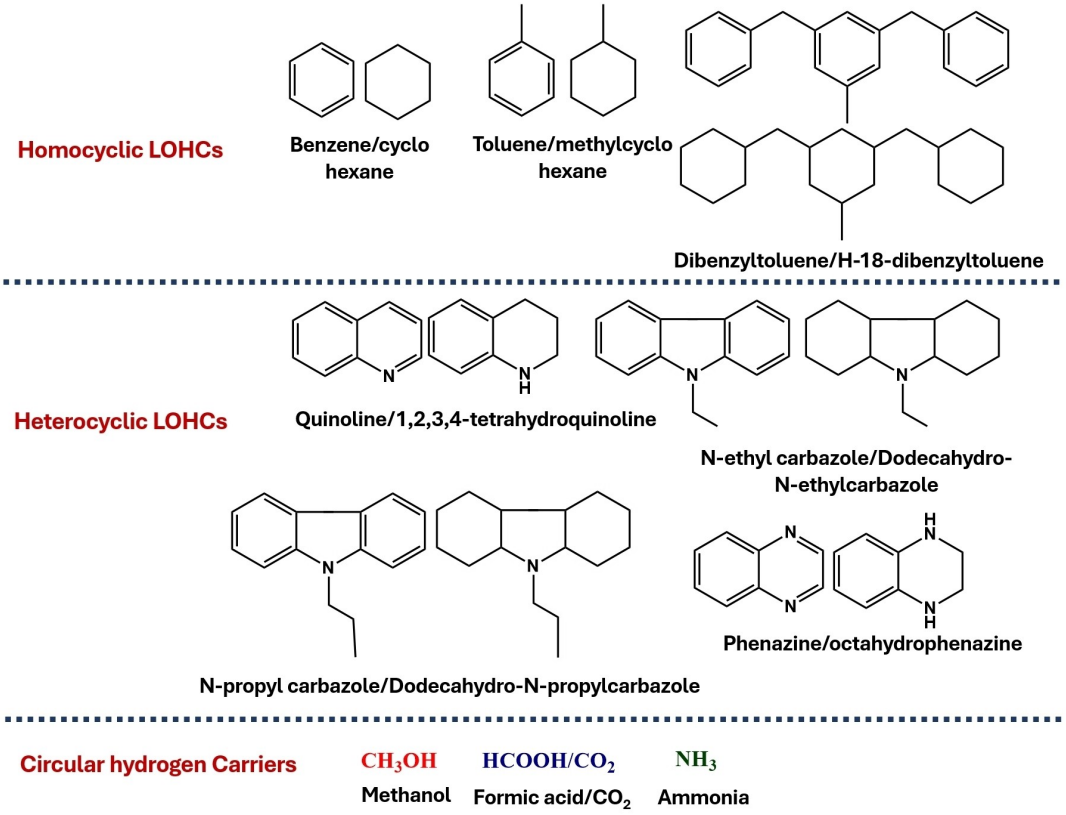

Figure 2. Important homocyclic and heterocyclic LOHCs.

genic toxicity of their dehydrogenated byproducts. According to calculations by Pez et al., the replacement of the carbon atom in a polycyclic aromatic compound with any hetero atom, such as N, S, or O brings down the enthalpy of hydrogenation to 62.8 kJ/mol.[19,38,39] These heteroaromatic compounds were found to be suitable for dehydrogenation at temperatures below 523 K. Among the N-heterocycles, dodecahydro-N-ethylcarbazole/N-ethyl carbazole (12-H-NEC/NEC), 1,2,3,4-tetrahydrquinoline/quinoline and dodecahydro-N-propyl carbazole/N-propyl carbazole (12-H-NPC/NPC) are the most detailed studied potential LOHC systems.[40–46] Other N-heterocyclic LOHC systems like 2-methyl indole, have also been explored and reported.[47] Circular hydrogen carriers, such as formic acid/formaldehyde, methanol/, and ammonia, are irreversible systems that release hydrogen along with byproducts like CO_2 and N_2 during dehydrogenation.[23,48,49] Formic acid, with a hydrogen storage capacity of 4.4 wt%, has been studied for dehydrogenation using both homogeneous (Fe, Mn, Ir) and heterogeneous catalysts (Pd, Co).[20,23,24,48,49] During the dehydrogenation reaction, dehydration of formic acid could lead to the release of CO, while the reverse reaction, hydrogenation, formic acid is regenerated from H_2 and CO_2. Studies by Olah and colleagues demonstrated reversible dehydrogenation and hydrogenation of formic acid using a Ru-trans dihydride complex with an aliphatic PNP pincer ligand.[50] Ammonia, with a gravimetric energy density of 17.5 wt%, is a promising circular hydrogen carrier; however, its derivatives such as amides, urea, and amine boranes are preferred due to the safety and the toxicity concerns associated with ammonia. Methanol, the simplest alcohol is another potential chemical energy carrier with a hydrogen storage capacity of 12.6 wt%. Akin to methanol, ethanol is another potential hydrogen carrier. It is non-toxic, inexpensive, and can be produced from biomasses such as sugarcane, corn, and grains.[51] Table 1 provides information on the hydrogen storage capacity of selected LOHC systems along with their reaction enthalpies.

3. Thermodynamics and Kinetics of Reversible Hydrogen Storage of LOHC Systems

The thermodynamics and kinetics of the LOHC systems are crucial for their effectiveness as hydrogen carriers. Dehydrogenation reactions typically demand a considerable input of heat as they are generally endothermic. In contrast, hydrogenation reactions release heat and are typically exothermic. The entropy change for hydrogenation reactions usually falls within the range of -130 to $-110\ JK^{-1}\ (mol\,H_2)^{-1}$ under standard conditions (298.15 K and 1 bar pressure). According to the free energy Equation (1), the free energy value is approximately 36 kJ $(mol\,H_2)^{-1}$ greater than the enthalpy value. Since hydrogenation reactions are generally exothermic (e.g., -68.7 kJ $(mol\,H_2)^{-1}$ for benzene), they can occur readily at room temperature. To facilitate the dehydrogenation/hydrogenation processes, it is advantageous to select compounds with an enthalpy of hydrogenation around -40 kJ $(mol\,H_2)^{-1}$ or slightly lower. If a compound's hydrogenation enthalpy is significantly lower than this threshold, dehydrogenation would necessitate higher temperatures for initiation. Conversely, for hydrogenation to be feasible, temperatures below 293 K would be necessary if the enthalpy exceeds this value, potentially resulting in sluggish reaction kinetics.[55]

$$\Delta^R G = \Delta^R H - T\Delta^R S \quad (1)$$

Cyclic hydrocarbons are generally known for their high dehydrogenation enthalpy, which limits most of their applica-

Table 1. Comparision of the physical properties of selected LOHC systems.

LOHC system	H_2 storage capacity	Enthalpy difference (kJ/mol H_2)	Boiling point (°C)		Melting point (°C)		References
			H_{lean}	H_{rich}	H_{lean}	H_{rich}	
Cyclohexane/Benzene	7.2	68.6	80	81	5.5	7	[14]
Methylcyclohexane/Toluene	6.2	68.3	111	101	−95	−127	[14,22]
Decalin/naphthalene	7.3	66.4	218	196 (cis)/ 187 (trans)	80	−43 (cis)/ −30 (trans)	[14]
H18-Dibenzyltoluene/dibenzyltoluene	6.2	62.0	390	371	−39/ −34	< −50	[14,22]
Bicyclohexyl/biphenyl	7.1	67.0	255	228	70	4	[10,14]
Dodecahydrocarbazole/carbazole	6.7	51.1	355	264	246.3	58	[10,20,52]
Dodecahydro- N-propylcarbazole/N-propylcarbazole	5.5	–	336	NA	48	NA	[10,53]
2-methyloctahydro indole/2-methyl indole	5.8	51.5	273	205	60	25	[54]
Dodecahydro- N-ethylcarbazole/N-ethylcarbazole	5.8	53.2	378	281	68	−84	[52,55]
Formic acid/CO_2	4.4	31.2	–		–		[23,24]
Ammonia	17.8	30.8					[56]
Methanol	12.5	63.9					[23]
Ethanol	4.3	–					[57]

tions. Wasserchied's studies demonstrated the effectiveness of oxygen-containing compounds, like benzophenone/dicyclohexylmethanol, as hydrogen carriers, exhibiting low dehydrogenation temperature and exceptional hydrogen storage capacity (7.19 wt%).[58] The alumina-supported Ru, Pt, and Pt/C catalysts were tested for hydrogenation of benzophenone. The reaction with Ru/Al_2O_3 showed high selectivity (98%) for perhydro-benzophenone (H14-BP) at 363 K. The same Ru catalyst facilitated the dehydrogenation of perhydro-benzophenone (H14-BP) to dicyclohexylketone (H12-BP) at 503 K, with a selectivity of 96%.[58] Additionally, to shed further light on optimizing the thermodynamics of LOHCs, investigations on the impact of introducing methoxy substituents with varying substitution positions on the quinoline and pyridine rings were conducted (Scheme 1).[59]

The studies demonstrated a significant dependence of substitution position on the enthalpy: substituents at the 2- and 4-positions led to a decrease in the enthalpy, while substitution at the 3-position resulted in higher enthalpic values (Tables 2 and 3). The liquid phase reaction enthalpy values, $\Delta_rH_m^0$ for

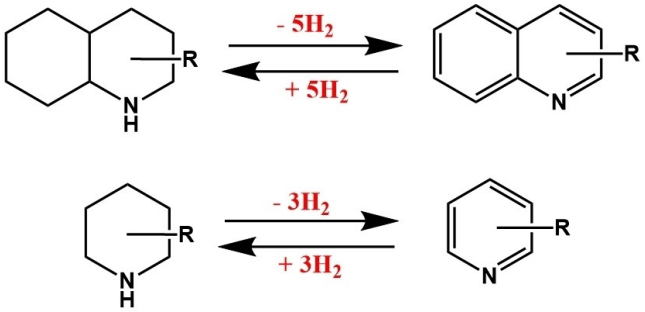

Scheme 1. Reversible dehydrogenation/hydrogenation of substituted pyridines and substituted quinolines. Adapted from Ref. [59] Copyright (2024) with permission from Wiley-VCH.

methoxy-substituted quinolines and pyridines ranged from 52.6 to 62.2 kJ/mol·H_2, depending on the specific site of substitution. The substitutions at the 2-position consistently yielded lower enthalpic values compared to the other substitution positions in both pyridines and quinolines. A notable trend was that, as the distance of the substituent from the nitrogen atom increased, enthalpy values and consequently, the equilibrium temperature tend to increase. On the other hand, methyl substitutions on pyridine and quinoline rings appeared to have minimal impact on the enthalpy values. When comparing methoxy and methyl substitutions, the former consistently exhibited lower enthalpies. While, it is feasible to reduce the enthalpy by employing a substituent, it is important to consider that such modifications may also lead to the formation of side products during reactions, as well as a decrease in gravimetric storage capacity.

Pez et al. in a series of patents proposed replacing carbon atoms with heteroatoms in cyclic hydrocarbons to reduce aromaticity, leading to a lowering in the enthalpy of dehydrogenation in the heterocyclic compounds like dodecahydro-N-ethylcarbazole and N-ethyl carbazole.[19,38,39] The same was supported by Crabtree by computational methods.[60] For instance, the dehydrogenation/hydrogenation enthalpy of H12-NEC/NEC is -50.5 ± 0.8 kJ/mol compared to that of decalin which is much higher.[13,55] These compounds exhibit lower enthalpy energy requirements (51–56 kJ/mol H_2) compared to cycloalkanes, with H_2 storage capacities of 4–6 wt%. However, their high melting points pose a limitation.[51] Attempts were made to reduce the melting points of the system by increasing the alkyl chain length which also resulted in a reduction of the H_2 storage capacity.[61] Binary mixtures of N-alkyl carbazole have been proposed to lower the melting points without compromising on the H_2 storage capacity.[61]

Table 2. Liquid phase reaction enthalpies, $\Delta_rH_m^0(liq)/H_2$ of the dehydrogenation of substituted pyridines.[59]

	$\Delta_rH_m^0(liq)/H_2$ (kJ/mol)		$\Delta_rH_m^0(liq)/H_2$ (kJ/mol)
Pyridine	62.2		
2-methoxy-pyridine	53.9	**2-methyl-pyridine**	60.5
3-methoxy-pyridine	60.4	**3-methyl-pyridine**	61.8
4-methoxy-pyridine	56.4	**4-methyl-pyridine**	60.9

Table 3. Liquid phase reaction enthalpies, $\Delta_rH_m^0(liq)/H_2$ of the dehydrogenation of substituted quinolines.[59]

	$\Delta_rH_m^0(liq)/H_2$ (kJ/mol)		$\Delta_rH_m^0(liq)/H_2$ (kJ/mol)
Quinoline	61.5		
2-methoxy-quinoline	52.6	**2-methyl-quinoline**	59.5
3-methoxy-quinoline	58.9	**3- methyl-quinoline**	60.7
4-methoxy-quinoline	56.0	**4- methyl-quinoline**	60.2
5-methoxy-quinoline	60.2	**5- methyl quinoline**	61.0
6-methoxy-quinoline	57.6	**6- methyl-quinoline**	60.4
7-methoxy-quinoline	57.9	**7- methyl-quinoline**	60.7
8-methoxy-quinoline	61.1	**8- methyl-quinoline**	60.7

Recent research has been directed towards investigating different types of LOHCs and the catalysts employed to facilitate hydrogen release and uptake. Numerous studies have been focused on the dehydrogenation of LOHCs using noble metal-based and transition metal nanoparticles under heterogeneous conditions.[21–23] Additionally, there are reports on the dehydrogenation and hydrogenation reactions of various LOHC systems using transition metal pincer complexes in homogeneous media.[62,63] However, most catalysts studied to date are specific to either dehydrogenation or hydrogenation reactions, rather than performing both simultaneously. Currently, significant attention is directed towards researching systems capable of performing both dehydrogenation and hydrogenation reactions reversibly using the same catalysts. Overcoming the challenge of finding affordable and efficient catalysts capable of performing both tasks is crucial for the widespread adoption of LOHCs.

This review focuses specifically on the solid heterogeneous catalysts showing promise for reversible dehydrogenation and hydrogenation using a single catalyst in a single vessel. Utilizing a single catalyst not only streamlines the processes but also offers economic and practical advantages. These catalysts are selected for their practicality, durability at high temperatures, and recyclability. The study explores various hybrid catalysts, including those consisting of a single metal, bimetallic, or pincer complexes immobilized on solid supports, all of which show potential for performing reversible hydrogen release and uptake in a single container.

4. Homogeneous Reversible Dehydrogenation/hydrogenation of LOHCs

Before the discussion on the use of a single heterogeneous catalyst for the dehydrogenation/hydrogenation reactions of LOHCs for hydrogen storage, a brief survey of some of the single homogeneous catalysts that have been explored in this domain will be covered (Figures 3 and 4). A significant emphasis has been placed on pincer complexes emerging as particularly promising candidates[44–46,48,64–67] These molecular organometallic catalysts offer the potential for operating under mild reaction conditions (typically in the range of 393 K–443 K) while providing efficient reaction pathways. The reactions are commonly conducted using fixed catalyst bed reactors, batch reactors, continuous reactors, or membrane reactors.[68] Each of these reactor configurations offers unique advantages and

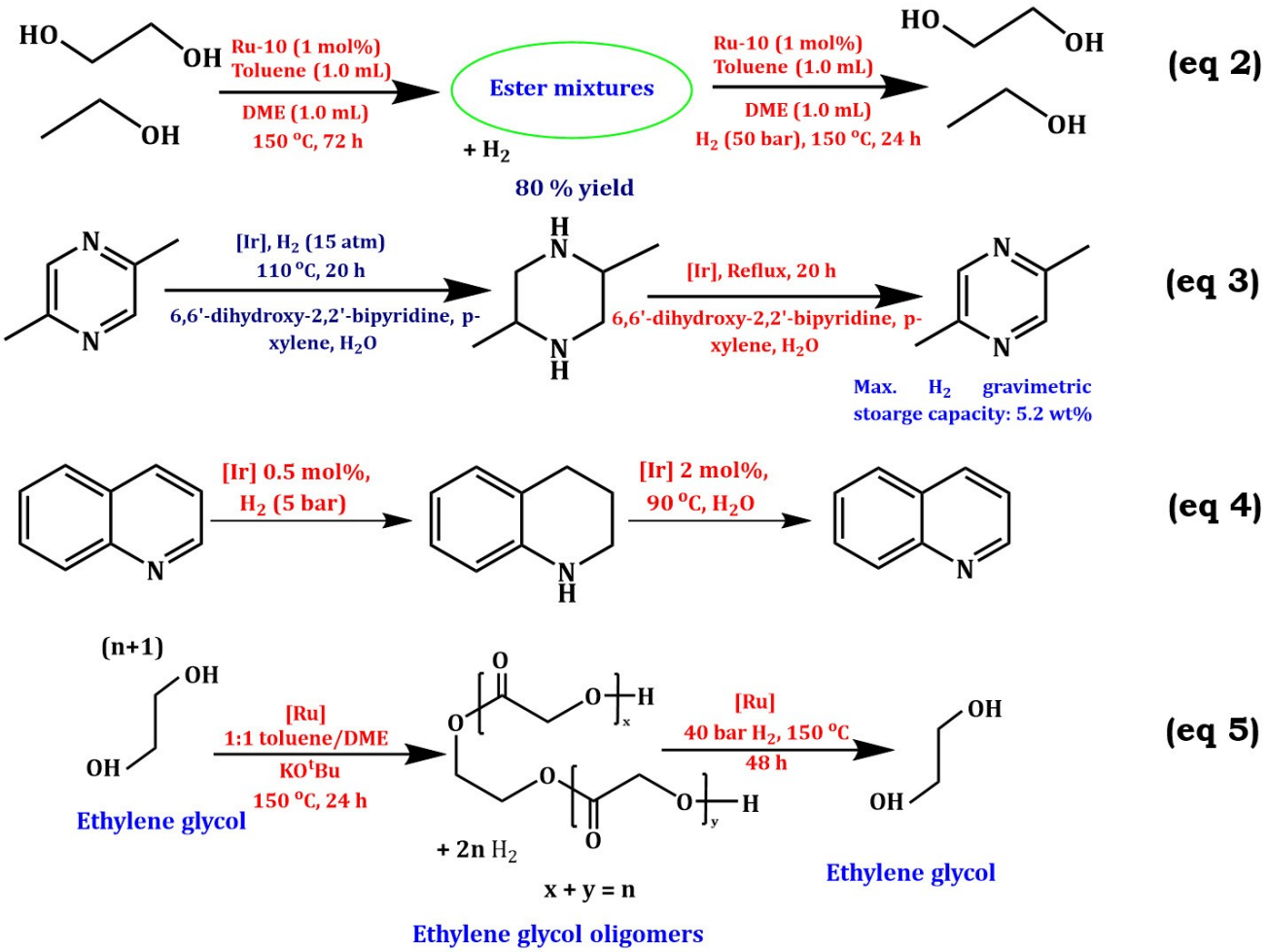

Figure 3. Selected homogeneous reversible dehydrogenation-hydrogenation reactions studied using homogeneous catalysts.[45,64–65,74]

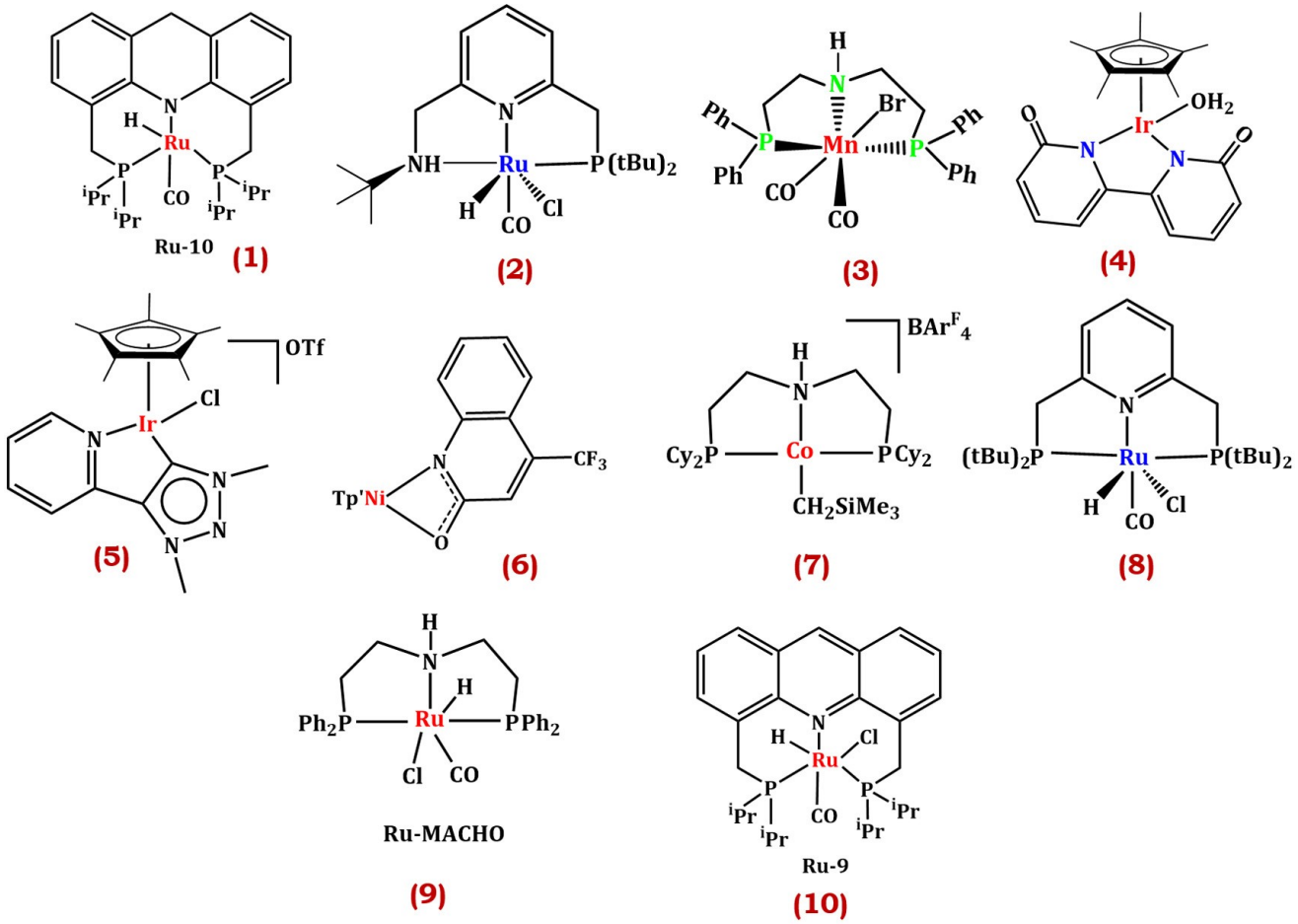

Figure 4. Selected homogeneous catalysts studied.[45–46,48,64–65,73–75,67]

challenges in the context of LOHC-based hydrogen storage systems.

The pioneering work of researchers such as Kaska, Jensen, and Koten has advanced the understanding in this area.[69–71] Pincer ligands, characterized by their secure binding to metal centers in a meridional geometry, contribute significantly to enhancing the thermal stability of the complexes.[72] Milstein et al. reported the use of a Ru PNP-type pincer complex (**1**) for reversible dehydrogenative esterification of ethylene glycol and ethanol, yielding a mixture of esters at 423 K. Under 50 bar H_2 pressure at 423 K, total recovery of the starting materials was achieved (Equation 2).[65] They also demonstrated reversible dehydrogenation-hydrogenation of 2-aminoethanol using a Ru pincer complex (**2**), achieving a hydrogen capacity of 6.6 wt%.[73] The dehydrogenation of amino ethanol took place under mild conditions (378 K–408 K), while the hydrogenation of the cyclic glycine anhydride proceeded at 383 K, 60 bar H_2. This approach opened up avenues for future advancements in pincer chemistry. Rueping and colleagues studied the base-catalyzed dehydrogenation and hydrogenation of N-heterocycles, utilizing a Mn-PNP pincer complex (**3**).[67] Their findings showcased outstanding catalytic activity coupled with high chemoselectivity. In another study, Shiraishi introduced an iridium-based complex (**4**) tailored for the reversible interconversion of 2,5-dimethylpyrazine/2,5-dimethyl piperazine, with a theoretical H_2 storage capacity of 5.2 wt% (Equation 3).[74] Remarkably, the catalyst exhibited exceptional conversion rates under mild conditions, achieving nearly 100% for both dehydrogenation and hydrogenation across multiple catalytic runs. Albrecht and team harnessed a triazole-based iridium complex (**5**) to investigate the reversible dehydrogenation-hydrogenation of quinolines and their derivatives within an aqueous medium, yielding promising results (Equation 4).[45] Jones et al. introduced tris(3,5-dimethylpyrazolyl)borate and 2-hydroxyquinoline ancillary ligand-supported Ni complexes for the reversible acceptorless dehydrogenation and hydrogenation of alcohols (**6**), showcasing their versatility in catalysis.[75] Furthermore, they also explored the acceptorless dehydrogenation and hydrogenation of N-heterocycles using cobalt pincer complexes (**7**), adding to the pool of efficient catalytic systems.[46] Pidko et al. utilized Ru-PNP pincer complex for reversible hydrogen storage, focusing on circular hydrogen carriers formic acid/CO_2, thus expanding the scope of hydrogen storage methodologies (**8**).[48] Lastly, Stavila et al. investigated {bis[2(diphenylphosphino)ethyl]amine} carboynlchlorohydridoruthenium(II) (Ru-MACHO) (**9**) and chlorocarbonylhydrido[4,5-bis-(di-*i*-propylphosphinomethyl)-acridine]ruthenium(II) (Ru-9) (**10**) catalysts for the dehydrogen-

ation/hydrogenation studies of polyols, ethylene glycol, and 1,2-propanediol, shedding light on their potential applications in sustainable chemical processes (Equation 5).[64]

While homogeneous catalysts offer advantages such as high diffusion rates, well-defined activities, and tunability, their use with expensive metals would be cost-prohibitive on a large scale and lacking in recyclability. Heterogeneous catalysts, on the other hand, address these challenges by facilitating recycling and recovery of the catalyst, thus reducing the costs and increasing sustainability. Heterogeneous catalysts are important in industrial settings for their ability to enhance thermal stability, as a result of their improved dispersion. These features of heterogeneous catalysts ensure consistent performance over multiple cycles, a crucial requirement for industrial applications.

5. Heterogeneous Reversible Dehydrogenation/hydrogenation of LOHCs

Several hybrid catalysts have been developed and investigated for reversible hydrogen storage reactions, utilizing a range of noble metals, transition metals, and occasional exploration of pincer complexes (Figure 5). Predominantly studied precious metals include Pd, Pt, and Au, as well as other transition metals such as Co and Ni, alongside iridium pincer complexes. This section of the review will include a discussion on dual functional catalysts explored for reversible hydrogen storage of cyclic hydrocarbon systems, where both monometallic and bimetallic noble metal catalysts and transition metal catalysts will be described. Following this, monometallic, bimetallic, and pincer-based catalysts for the nitrogen-based heterocyclic systems and circular hydrogen carriers will be discussed.

5.1. Reversible Dehydrogenation/hydrogenation of Cyclic LOHC Hydrocarbon Systems

5.1.1. Monometallic Catalysts

Studies on reversible hydrogen storage using LOHCs have been focussed on cyclic hydrocarbons because of their high energy storage capacity, high boiling point, and stability. However, the implementation of these hydrocarbons has not been feasible primarily due to the endothermicity of the reaction. Kustov and his team researched Pt and Pd-based catalysts supported on various materials (Al_2O_3, SiO_2, C, Sibunit), and evaluated their performance for the hydrogenation and dehydrogenation of terphenyl and tercyclohexane.[76–78] Among the catalysts tested, the 5% Pt/SiO_2 catalyst exhibited the highest terphenyl conversion for hydrogenation, while the 10% Pt/C catalyst showed superior dehydrogenation activity under unstirred reaction conditions. However, under stirring conditions, the

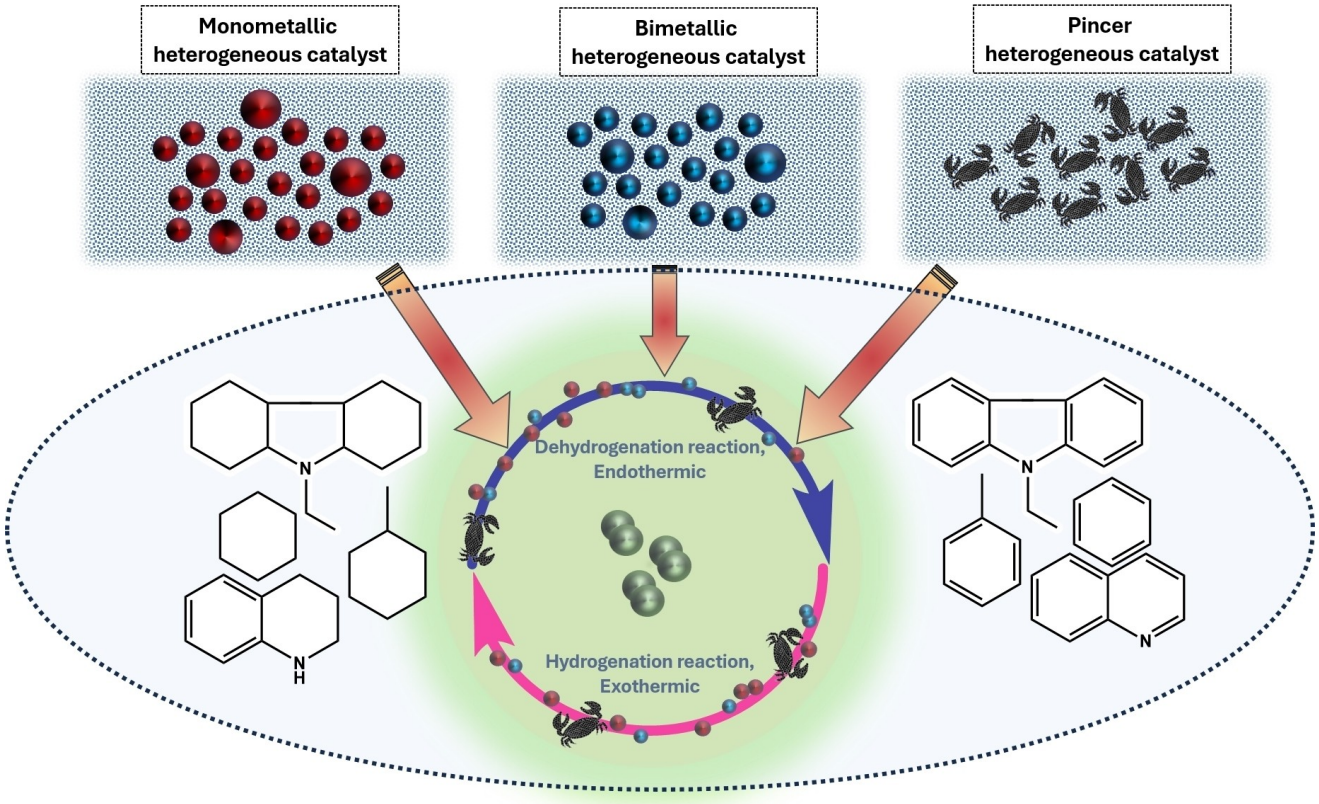

Figure 5. Demonstration of reversible heterogeneous dehydrogenation/hydrogenation reactions on different single hybrid catalysts.

10% Pt/C catalyst displayed excellent activity for both dehydrogenation and hydrogenation, with a hydrogen consumption of 7.8 wt% for terphenyl hydrogenation and a hydrogen release capacity of 7.25 wt%. Additionally, they explored the impact of the isomerization of o-terphenyl on dehydrogenation and hydrogenation using 3 wt% Pt/C. Their studies revealed the formation of certain isomers (m-terphenyl and triphenylene) which led to a decrease in the overall reaction rate[77] The group also compared the catalytic reversible dehydrogenation-hydrogenation performance of these catalysts for perhydro-meta-terphenyl/meta-terphenyl systems (Table 4).[78] For this system, a 3% Pt/C catalyst was found to show a faster rate of hydrogenation compared to the alumina-based catalysts, which could be due to the diffusion restrictions as a result of the pore-clogging of alumina with coke. The time required for the hydrogenation reaction was found to be the same for both Pt/C and Pt/Sibunit, despite the fact that the latter had twice the smaller surface area than the former (Table 4, entries 4 and 5).

Kustov's group extended the work on the same system investigating the impact of specific intermetallic compounds, such as Mg_2Ni and $LaNi_5$, both undoped and doped with Pt (Table 5).[79] Their research unveiled remarkable results, notably achieving nearly 100% conversion with no hydrogenolysis products using the catalyst 1% Pt/Mg_2NiH_x. Moreover, they observed that the reaction rate was influenced by both temperature and the percentage loading of the noble metal. Notably, the hydrogen release rate doubled, reaching 26 cm^3/min for the 5% Pt catalyst at 613 K.

In the year 2015, Aslam and co-workers studied the dehydrogenation and hydrogenation of the methylcyclohexane/toluene (MCH-Tol) system, an important LOHC from a practical application point of view, using 1 wt% Pt/zeolite beta catalyst.[29] The catalyst was prepared using an ion exchange process and the studies were carried out in a fixed-bed tubular reactor. The reversible reactions proceeded with the formation of byproducts, ethyl cyclopentane, and isomers of dimethyl cyclopentane. The authors also demonstrated the effect of temperature and pressure on the percentage conversion of the reactants and the byproduct formation. At 1.013 bar pressure, the overall conversion was found to increase however, the yields of the by-products decreased with the increase in the hydrogen concentration in the feed.

Table 4. Catalytic activity of different catalysts for *meta*-terphenyl hydrogenation and perhydro-*meta*-terphenyl dehydrogenation.[78]

Catalyst	Surface area (m^2/g)	Hydrogenation (%)	Dehydrogenation (%)
5% **Pt/Al_2O_3**	230	99	43
2.5% **Pd/Al_2O_3**	215	73	35
0.12%**Pd-3**.8%**Ni-4**.3% **Cr/Al_2O_3**	130	86	26
3% **Pt/C**	760	100	92
3% **Pt/Sibunit**	300	99	91

Table 5. Comparison of the rate of hydrogen release of perhydroterphenyl system using Pt/Mg_2NiH_x catalyst at different loading and different reaction temperatures. Adapted from Ref. [79] Copyright (2013) with permission from Elsevier.

Catalyst	Dehydrogenation temperature, K	Rate of hydrogen release, cm^3/min
1% **Pt/Mg_2NiHx**	593	4.0
1%**Pt/Mg_2NiHx**	613	7.2
5% **Pt/Mg_2NiHx**	593	10.5
5% **Pt/Mg_2NiHx**	613	25.8

In 2015, Li and colleagues demonstrated a reversible hydrogen storage system utilizing a cyclohexane/benzene reaction facilitated by Pt/TiO_2 catalysts.[80] This study employed visible light radiation alongside noble metal nanoparticles, including Au, Pt, Pd, Ir, and Ru, supported on TiO_2, specifically focusing on $Pt@TiO_2$ produced through a chemical reduction method. In addition to TiO_2, the researchers also investigated GaN and Al_2O_3 as supports for cyclohexane dehydrogenation. They determined that 5 wt% of $Pt@TiO_2$ nanoparticles yielded the best results, achieving nearly 99% conversion of cyclohexane with 100% selectivity for benzene. The hydrogenation process also showed impressive results, with a 97% conversion rate. The active site for the dehydrogenation was identified as metallic Pt, whose electrons, when excited by visible light, interact with the antibonding C–H orbitals to effectively cleave the C–H bonds.

Another LOHC system, H18-dibenzyltoluene/H0-dibenzyltoluene (H18-DBT/H0-DBT) is the most recently studied, having the advantages of being non-toxic and non-explosive, liquid at room temperature, possessing high hydrogen storage capacity.[22] Wasserscheid et al. reported the Pt/alumina catalyst for stationary hydrogen and energy storage using a hot-pressure swing reactor.[81] Reversible reactions were performed in a single reactor with 0.025 mol% catalyst for hydrogenation showing good activity with full conversion at 30 bar hydrogen pressure and temperatures above 564 K, followed by dehydrogenation at the same temperature. The catalyst was tested for 4 dehydrogenation-hydrogenation cycles, and a hydrogen loading capacity of 4.6 mass% hydrogen was obtained. After the first cycle, a significant decrease in the dehydrogenation-hydrogenation productivity was noted, following which further cycles exhibited low catalyst deactivation. The reactor was constantly maintained at an elevated temperature for both processes, making the dehydrogenation-hydrogenation processes faster. To create a boundary condition and make use of the heat generated during the exothermic hydrogenation reaction for the subsequent endothermic dehydrogenation sequence, a slightly high temperature for the hydrogenation reaction was employed, 583 K, maintaining a temperature difference of 283 K. The study, although for stationary hydrogen storage, makes the entire process of the hydrogen storage system, simpler and cost-effective.

The same system was also explored by Yang and co-workers using the same catalyst in a single reactor simplifying the entire process.[31] The authors evaluated different parameters to optimize the reaction conditions. From the effect of temperatures on the dehydrogenation-hydrogenation reactions, 413 K

and 543 K were particularly found to be the optimal hydrogenation and dehydrogenation temperatures, respectively. Next, they studied the influence of various supports (Al_2O_3, HAP, SBA-15, C) on the hydrogenation-dehydrogenation reaction and also tested different wt% of Pt loading on the supports (Table 6). The Al_2O_3 support was found to be the best one with a metal loading of 3% being the optimal, considering both, dehydrogenation and hydrogenation reactions. Cyclic hydrogen storage tests were conducted over 5 cycles, with the hydrogenation capacity decreasing and hydrogen storage efficiency increasing as the cycle proceeds.

Further in 2020, Yi et al. investigated the H18-DBT/H0-DBT system with a 3% Pt/alumina catalyst.[82] They investigated the impact of plasma treatment using oxygen and hydrogen on the catalytic performance of the alumina catalysts. The 3% Pt/Al_2O_3-P-O_2 catalyst showed high hydrogen uptake as a result of hydrogen spillover, the extent of which was dependent on the surface hydroxyl vacancies. An increase in the surface hydroxyl groups as a result of oxygen treatment, not only increased the extent of hydrogen spillover on the catalyst but also boosted the catalyst performance in dehydrogenation and hydrogenation and prevented side reactions. Conversely, hydrogen treatment increased oxygen vacancies, along with an increase in the portion of low-coordinated Pt sites. These low-coordinated Pt sites are not active for the dehydrogenation reaction. Therefore, to consider the long-term performance of DBT as a potential LOHC, a delicate balance between the increased surface hydroxyl groups and decreased surface oxygen vacancies on the Pt/Al_2O_3 is to be maintained.

Kustov and co-workers further studied the impact of steric factors on the reversible dehydrogenation-hydrogenation processes in fused polyaromatic hydrogen storage systems (benzene, naphthalene, and anthracene) and linearly linked polyaromatic compounds (biphenyl, para-, meta-, and ortho-terphenyl).[83] Their findings revealed that the hydrogenation rate is influenced by both, thermodynamic stability and destabilization energy of the aromatic system. Interestingly, steric effects were more pronounced in the later stages of the hydrogenation process. Moreover, the reverse dehydrogenation process was found to be dependent on the structural configuration and degree of condensation within the polycyclic system under investigation. Considering the diverse kinetic parameters, the biphenyl/bi-cyclohexyl pair emerged as the optimal hydrogen storage system.

Table 6. Reversible dehydrogenation-hydrogenation of H18-DBT/H0-DBT using Pt supported on different supports.[31]

Catalyst[a]	Dehydrogenation[b] % after 300 min	Time taken for complete hydrogenation[c] (min)
5% Pt/Al_2O_3	56.3	35
5% Pt/HAP	27.7	100
5% Pt/SBA-15	34.2	60
5% Pt/C	58.2	280

[a] Pt/H0-DBT molar ratio 0.3 mol%; [b] Dehydrogenation conditions: 543 K, atmospheric pressure; [c] Hydrogenation condition: 3–4 MPa, 413 K.

In the same year, Xie et al. reported nano-Pd/CeO_2 catalysts for reversible vapor phase dehydrogenation-hydrogenation reactions of cyclohexane/benzene.[84] The authors explored different synthetic procedures for preparing CeO_2 and tested the respective catalysts for reversible hydrogen storage (Table 7). The synthesis of the Pd/CeO_2-HT catalyst, via the wet-impregnation method, involved KIT-6 as a template providing a 3D mesoporous structure for CeO_2 preparation. An enhanced hydrogenation activity of the Pd/CeO_2-HT catalyst was noted which was attributed to several factors like high surface area, exposure of the highly active {110} planes of CeO_2, and the high dispersion of Pd. The role of metallic Pd was attributed to its ability to activate H_2 molecules, whereas the activation of benzene was facilitated by the oxygen vacancies present on the CeO_2 support. These characteristics collectively enabled efficient adsorption, migration, diffusion, and desorption of the reactant molecules within the catalyst pores, thereby facilitating superior hydrogenation activity. The catalyst demonstrated remarkable performance, achieving >99% with 100% selectivity at 473 K for benzene conversion during hydrogenation, and up to 65% cyclohexane conversion with complete selectivity towards benzene and H_2 at 723 K during dehydrogenation.

Another CeO_2-supported catalyst that was explored was Pt_1/CeO_2 for the reversible dehydrogenation/hydrogenation of the methylcyclohexane/toluene system.[27] The Pt catalysts are isolated single atoms which displayed excellent catalytic performance (309-fold higher) and good selectivity in comparison to the traditionally supported Pt nanoparticles. This was attributed to the super synergistic effects between Pt and CeO_2. The benzene-cyclohexane system was also explored by Xie and co-workers, using a Pd/γ-alumina catalyst with 1.0 wt% metal loading and HNO_3 as a promoter.[28] Vapor phase hydrogenation of benzene afforded 97.51% conversion and 100% selectivity at 473 K and atmospheric pressure, using the 1PAN15 catalyst (prepared using 1.5 HNO_3/H_2O impregnation volume). The Pd atoms served as active sites, transferring electrons from their outer d-orbitals and accepting electrons from H_2, to form Pd–H bonds during hydrogenation. Dehydrogenation takes place at

Table 7. Comparision of the catalytic performance of different Pd/CeO_2 catalysts for cyclohexane and benzene production.[84]

Catalysts	Surface area[a]	Hydrogen production (g/h)	$C_{benzene}$ (%)[b]	$C_{cyclohexane}$ (%)[c]
Pd/CeO_2-HT	107.8	73.77	99.5	65.3
Pd/CeO_2-ST	69.7	70.59	98.8	62.5
Pd/CeO_2-HY	71.6	62.04	96.4	55.1
Pd/CeO_2-PC	57.7	60.85	95.6	54.5
Pd/CeO_2-CA	33.4	51.48	86.0	45.5

$C_{benzene}$ and $C_{cyclohexane}$ (%): The conversion of benzene and cyclohexane respectively; Both reactions exhibited 100% selectivity. [a] Calculated from BET formula; [b] Hydrogenation reaction carried out at temperature 473 K under atmospheric pressure and gas mass space velocity of 12,000 mL h^{-1}, feed gas benzene and H_2 with a volume ratio of 1:30; [c] Dehydrogenation reaction carried out at temperature 723 K and gas mass space velocity of 12,000 mL h^{-1}

473 K–723 K, with the 1PAN15 catalyst bringing about 90.9% conversion at 673 K and resulting in the production of 6.54 wt% hydrogen.

5.1.2. Bimetallic Catalyst

Bimetallic catalysts in the form of alloys, heterostructures, or intermetallic compounds have demonstrated significant advantages over the monometallic counterparts.[85] The enhanced catalytic performance of the bimetallic catalysts has been ascribed to the synergistic interplay between the two constituent metals. The incorporation of a second metal could facilitate the enhancement of both the selectivity and the stability of the catalyst. For instance, Lindlar's catalyst (Pd–Pb) exhibits improved selectivity, while the addition of Au to Pd enhances the catalyst's resistance towards sintering.[85] Pt-based catalysts are well-known for their high catalytic activity; however, they are particularly susceptible to CO poisoning. Research on the Pt_8 cluster has shown that substituting one Pt atom with Ru reduces CO poisoning effects.[86] Incorporation of a second metal induces a shift in the d-band center towards the Fermi level due to charge polarization in the Ru_1Pt_7 system, resulting from the difference in electronegativity between the two metals. This shift enhances the adsorption capabilities for both O_2 and CO activation.

Another important consideration is the immobilization of metals on support materials, which could significantly affect the electronic and geometric structures of the catalyst system. For example, when Pt atoms are immobilized on SnO_x/TiO_2 a Pt–Sn bond is formed as SnO_x gets reduced to metallic Sn and Ti^{+3} gets oxidized to Ti^{+4}.[87] The dipole-dipole repulsion resulting from electron transfer from Sn to TiO_2 effectively prevents sintering by inhibiting the agglomeration of the Pt–Sn clusters. Within supported bimetallic catalysts, variations in size, from binuclear metal sites to nanoclusters to nanoparticles, also influence the reactivity, behavior, and stability, as evidenced in the Pt–Sn system.[88]

The electronic properties of the bimetallic systems depend on multiple factors, including particle size, composition, interactions with the support, and the coordination environment. Although the exact mechanisms behind the synergistic effects that enhance catalytic performance remain unclear, it is evident that these interactions are influenced by the geometric and the electronic arrangements of the two metals. Utilizing density functional theory allows for the consideration of parameters such as electron affinity, electronegativity, d-band center, and Mulliken charge, could elucidate the reactivity patterns of these catalysts. For example, in a study for the evaluation of electrocatalytic hydrogen evolution using a bimetallic Ni–Co system, variations in the second metal significantly altered the d-band center, thereby facilitating improved water dissociation activity.[85]

Guo and co-workers in 2020,[89] investigated the Cu–Pt bimetallic system supported on silicalite for methylcyclohexane/toluene dehydrogenation/hydrogenation. Under optimized conditions, they achieved impressive hydrogen evolution and storage rates, reaching 445.3 mmol g Pt^{-1} min^{-1} with 92.26% methylcyclohexane conversion and 1271 mmol g Pt^{-1} min^{-1} with 99.9% toluene conversion, respectively. The doping of Cu in Pt not only improved the dispersion of Pt but also enhanced the catalyst's resistance to coking.

A recent work by Jangir and Jagirdar demonstrated a tandem dehydrogenation/hydrogenation reaction using a single heterogeneous Pd–Ru/Ir/Al_2O_3 hybrid catalyst[90] (Figure 6). The catalyst is comprised of two components, a thermally stable iridium pincer complex which carries out the dehydrogenation reaction, whereas Pd–Ru nanostructures, bring about the hydrogenation reaction. To test the catalytic activity of the catalyst, cyclooctane/cyclooctene, a thermodynamically favorable system was chosen as a model substrate. The dehydrogenation was performed at 443 K, atmospheric pressure, while the hydrogenation reaction was carried out at room temperature and 1 atm H_2 pressure. This study opened a new avenue to design and develop tandem catalysts for investigating the hydrogen storage aspects of different LOHCs.

5.2. Reversible Dehydrogenation/hydrogenation of N-heterocyclic LOHC Systems

5.2.1. Monometallic Catalysts

Reversible hydrogen storage utilizing N-heterocyclic systems has garnered significant interest due to their impressive hydrogen storage capacity and lower dehydrogenation enthalpy when compared to cyclic hydrocarbons. Among these, the quinoline/1,2,3,4-tetrahydroquinoline system stands out as one of the most extensively researched heterocyclic systems. Kaneda and co-workers in the year 2011 reported heterogeneous copper nanoparticles supported on titania surface (Cu/TiO_2) for the reversible dehydrogenation/hydrogenation of tetrahydroquinoline/quinoline under mild reaction conditions.[91] The dehydrogenation reaction was scalable (tested upto 20 mmol) without compromise on the percentage conversion. Repeated cycles of dehydrogenation/hydrogenation were achieved with a negligible decrease in the percentage conversion.

In 2013, Gu et al. demonstrated remarkable catalytic activity for reversible hydrogenation and oxidative dehydrogenation of the N-heterocyclic systems using Pt wire catalyst.[92] The catalyst was prepared by acidic etching of FePt nanowires in the air. At

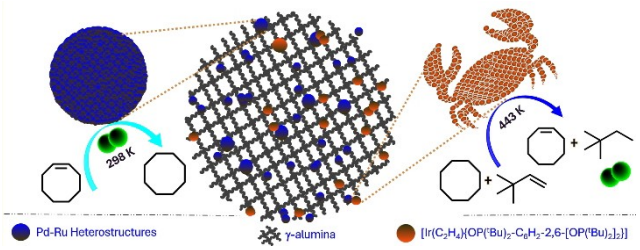

Figure 6. Schematic showing the tandem dehydrogenation-hydrogenation reaction by Pd–Ru/Ir/Al_2O_3 hybrid catalyst.

353 K and atmospheric hydrogen pressure, using this catalyst, 97.9% conversion and 94.1% selectivity were achieved for the hydrogenation of quinoline in water. Reversing the reaction to quinoline was achieved by a simple change in the atmosphere to oxygen or air, yielding >99% at 313 K and atmospheric pressure. The catalyst was evaluated for its activity in different solvents (H_2O, ethanol, chloroform, THF) and the yields were found to be modest. The binding of quinoline to the active Pt(111) was preferentially through the aromatic π-cloud. In the case of pyridine and substituted pyridines, the upright position of the substrate prevents the interaction with Pt(111), and therefore, lower conversions were reported in that case. The catalyst maintained its activity over 10 cycles without leaching.

In 2017, Li and colleagues, utilized Co nanoparticles encapsulated within N-doped graphene shells (NGS), Co@NGS for the demonstration of reversible hydrogen storage in N-heterocyclic systems.[93] The encapsulation strategy effectively prevented the leaching and aggregation of the nanoparticles, thereby boosting the catalytic performance. A synergistic effect was noted for the bifunctional catalyst, where the graphene shell-modified Co nanoparticles facilitate oxidative dehydrogenation via electron transfer, whereas the Co nanoparticles influenced by the N dopants, facilitate H_2 activation. Similarly, Somorjai used metal nanoparticles (Pd, Pt, Rh) stabilized by PolyAMido Amine (PAMAM) dendrimers, supported on SBA-15, for the reversible hydrogen storage of quinoline and indoline derivatives.[94] These air-stable, recyclable catalysts showed complete dehydrogenation at 403 K and hydrogenation at 293 K–333 K under 1 atm H_2 pressure. With a 5 wt% catalyst loading, all the metal nanoparticles/SBA demonstrated complete dehydrogenation of 2-methyl-1,2,3,4-tetrahydroquinoline to 2-methyl quinoline. Shimizu further developed a Pt/C catalyst for the tetrahydroquinoline/quinoline system with 100% conversion and 91% yield by refluxing the reaction under a nitrogen atmosphere.[95] The reverse reaction was conducted using the same catalyst at 433 K and 3 bar H_2 pressure affording 84% yield of the starting materials along with side products. The effectiveness of the platinum catalyst for the catalytic performance was attributed to the moderate d-band center, which is neither too deep (as in the case of Ag and Cu) nor too close (Ni, Co) to the Fermi level, facilitating favorable interaction. This moderate d-band center favors a moderate M–H bond strength which leads to the catalytic dehydrogenation of N-heterocycles.

Another area that has garnered a lot of attention in reversible hydrogen storage is single-atom catalysts (SAC). Li and co-workers in 2018, using Co on ordered N-doped carbon porous matrix (ISAS-Co-OPNC), studied the dehydrogenation and transfer hydrogenation of N-heterocycles.[96] Their catalyst demonstrated >99% conversion for the dehydrogenation of 1,2,3,4-tetrahydroquinoline in both air and under inert atmosphere. For the reverse reaction, hydrogenation of quinoline took place effectively using formic acid or external hydrogen as H_2 source, resulting in nearly 99% yield of 3,4-dihydroquinoline-1(2H)-carbaldehyde; this could easily be hydrolyzed using $NaOH/H_2O/EtOH$ to regenerate 1,2,3,4-tetrahydroquinoline. The catalyst showed recyclability for up to 6 runs without significant degradation.

Piperidines are another set of potential LOHCs characterized by high hydrogen storage capacity, abundance, and low cost. In 2019, Milstein obtained a palladium catalyst (Pd/C) using $Pd(OAc)_2$ as a precursor and activated carbon as support and studied the reversible dehydrogenation/hydrogenation of piperidine/pyridine derivatives.[97] The catalyst exhibited excellent activity for the two potential LOHCs, 2-picoline/2-methylpiperidines and 2,6-lutidne/2,6-dimethylpiperidine with theoretical hydrogen capacity of 6.1 wt% and 5.3 wt%, respectively. The dehydrogenation of 2-methyl piperidines yielded nearly 90% H_2 at 443 K after 51 h whereas, 2,5-dimethyl piperidine yielded 97% of H_2 after 13 h of reaction using 0.3 wt% Pd/C. The reverse reaction, hydrogenation, on the other hand, resulted in 100% yield of 2,6-lutidine at 1.6–5 bar H_2, 423 K in 18 h, and 90% yield of 2-picoline at 2–7 bar. When activated carbon with acidic groups was used to support the Pd catalyst, an enhanced catalytic dehydrogenation activity was observed. Similar systems were also investigated by Balaraman et al. for the reversible acceptorless dehydrogenation-hydrogenation using a Co-Phen@C catalyst.[98] The reaction was performed at 423 K under argon flow for dehydrogenation and at 393 K under a hydrogen atmosphere for hydrogenation. The catalyst was also suitable for other N-heterocycles like indole, isoquinoline, anthracene, and benzoquinoline. The acceptorless dehydrogenation reaction using the cobalt catalyst gave excellent results and was found to be independent of the electronic nature and sensitivity of the functional groups.

In another study, for the reversible hydrogen storage of quinoline, Chen et al. used a nitrogen-thermal modification approach to synthesize Co nanoparticles on a nitrogen-doped carbon matrix (Co_x/N_yC catalysts).[42] The hydrogenation and dehydrogenation were carried out at 5 bar H_2, 393 K, and 433 K respectively. The catalyst exhibited high performance with the basic sites on the matrix driving both dehydrogenation and hydrogenation; using the matrix alone, a yield of 32% dehydrogenation product was obtained. The addition of Co significantly improved the performance through synergistic effects. DFT calculations indicate that the nitrogen-doped matrix activated H_2 by aligning the Fermi level of Co closer to the antibonding state of the adsorbed hydrogen, facilitating H_2 dissociation.

Ma and colleagues employed a synthesis method involving multiple pyrolysis steps of dicyandiamide and cobalt(II) acetylacetonate to produce cobalt nanoparticles.[99] These nanoparticles were then encapsulated within N-doped carbon nanotubes (NCNTs). This encapsulation technique, combined with the synergistic interplay between the nanoparticles and NCNTs, resulted in good catalytic activity for both oxidative dehydrogenation and transfer hydrogenation of N-heterocycles. In this system, the NCNTs serve as active sites for oxidative dehydrogenation, facilitating the activation of O_2, while the cobalt nanoparticles function as active sites for transfer hydrogenation, enabling the activation of H_2. Importantly, these processes are mutually supportive through synergism. Specifically, electron transfer from cobalt enhanced the dehydrogenation reaction,

and the presence of doped nitrogen atoms in the carbon nanotubes played a crucial role in facilitating the overall catalytic activity.

Wu and colleagues developed a Pd/Al_2O_3-YH_3 catalyst for reversible dehydrogenation and hydrogenation in the 12H-NEC/NEC system.[100] The introduction of YH_3 enhances the reaction kinetics by creating new hydrogen transfer pathways. The active site for both hydrogenation and dehydrogenation is the Pd metal, which demonstrates strong adsorption affinity for the organic substrates and hydrogen atoms. By adding YH_3, a significant number of active sites are generated, reducing competition for adsorption between hydrogen and the organic substrates, thereby improving the catalytic activity. The catalyst remains stable over three cycles of reversible hydrogen storage, achieving a hydrogen storage capacity of 5.5 wt%.

Another study in 2021 focused on the reversible dehydrogenation-hydrogenation of 1,2,3,4-tetrahydroquinoline/quinoline using ruthenium phosphide nanoparticles supported on activated carbon, Ru_2P/AC.[101] The introduction of phosphorus into the catalyst system induces synergistic effects that intricately alter the spatial arrangement and electronic properties of the catalyst. Specifically, the presence of phosphorus likely promotes a rearrangement in the spatial configuration, leading to a subtle increase in the distance between the two ruthenium atoms. This adjustment facilitated an electron transfer process within the catalyst structure. Consequently, these modifications in both, electronic and geometric aspects, resulting from the synergistic interaction, played a pivotal role in enhancing the bifunctional properties and the activity of the catalyst. The catalyst showed good reusability over 8 cycles.

On the other hand, in the year 2023, Mata and colleagues focused on a single solid heterogeneous catalyst composed of Pd nanoparticles supported on reduced graphene oxide (rGO).[102] The rGO served a dual function, acting as a carbocatalyst and support for Pd nanoparticles. The synthesis involved using a N-heterocyclic carbene palladium molecular complex precursor, which interacts with the graphene support via a polyaromatic tag in the ligand. Upon decomposition of this complex on the support, Pd nanoparticles stabilized by ligands were formed. This hybrid catalyst exhibited bifunctional properties, with Pd nanoparticles serving as active sites for hydrogenation reactions while rGO acted as a carbocatalyst in the acceptorless dehydrogenation of N-heterocycles. The reaction's outcome was significantly influenced by various factors such as solvent choice and temperature conditions, highlighting the importance of reaction conditions in controlling the catalytic performance.

To further enhance the catalytic activity, Yang et al., studied a high surface area porous composite, CeO_2/Al_2O_3.[40] The composite was synthesized via a co-precipitation method and the catalyst, Pd/CeAl-n (n = theoretical weight percent of CeO_2 in CeO_2-Al_2O_3) was prepared via incipient wetness impregnation method.[40] The surface area of the 20 wt% CeO_2/Al_2O_3 was found to be 330 m^2/g and the corresponding palladium catalyst, Pd/CeAl-20 had a surface area of 287.2 m^2/g. The introduction of CeO_2 contributes to the enhanced performance of the catalyst by inducing better dispersion of Pd on the surface and providing a greater number of catalytically active sites. The interaction between Pd and CeO_2 was found to have a Pd–O–Ce structure leading to an electronic interaction between them which led to an enhanced catalytic activity. The catalyst demonstrated excellent reversible hydrogen storage in the N-propylcarbazole (NPCZ) system. The best hydrogen storage and release of the NPCZ system obtained was 100% in 180 min.

In 2023, An and colleagues developed a single-batch catalyst for reversible hydrogen storage using octahydro-N-methylindole/N-methylindole (8H-NMID/NMID). Their catalyst featured Pd loaded on hierarchical titanate nanosheets (HTN), synthesized through a urea-assisted deposition-precipitation method followed by reduction with $NaBH_4$.[103] The HTN, prepared via solvothermal synthesis, exhibited a high density of acidic sites and oxygen vacancies, which contributed to the catalyst's enhanced activity due to hydrogen spillover. The hydrogenation process was achieved up to 5.70 wt% hydrogen storage with over 99% conversion of NMID, while the dehydrogenation reaction released 5.46 wt% hydrogen. The catalyst demonstrated impressive stability, maintaining its catalytic activity across five cycles of reversible hydrogen storage in a single-batch reactor, with no observable structural or phase changes.

Recently, Jagadeesh and colleagues reported the preparation of Co nanoparticles, stabilized by various ligands and supported on hydroxyapatite (HAP).[104] They assessed the catalyst's efficacy in the dehydrogenation of THQ/quinoline and other substituted N-heterocycles. Interestingly, the choice of ligand for stabilization and the pyrolysis temperature during the synthetic process appeared to influence the activity of the catalyst significantly. The different ligands used for the stabilization of Co nanoparticles include terephthalic acid (TPA), piperazine (PZ), trimesic acid (TMA), pyromellitic acid (PMA), etc. along with different pyrolysis temperatures (873 K, 973 K, 1073 K, 1173 K, 1273 K). Among the different catalyst types examined, Co–Pz-TPA@HAP-800 emerged as the most active, yielding a remarkable 95% yield of the hydrogenated product. Additionally, the activity of the catalyst was influenced by the solvent used (Table 8), with the highest hydrogenation activity realized in water, while the dehydrogenation process exhibited the highest activity in non-polar solvents such as n-hexane. The

Table 8. Dehydrogenation and hydrogenation of quinoline/THQ using Co–Pz-TPA@HAP-800 in different solvents.[104]

Solvent	Hydrogenation Yield (%)	Solvent	Dehydrogenation Yield (%)
H_2O	99	**H_2O**	51
n–hexane	31	**n–hexane**	94
1,4-dioxane	38	**MeOH**	69
iPrOH	42	**CH_3CN**	54
iPrOH/H_2O	95	**m–xylene**	73
THF	57	**DMF**	62
Toluene	87	**Toluene**	61

study was also extended to other substituted heterocycles, and the catalyst retained its activity in the presence of functional groups. In recent work, Wang and colleagues introduced a cost-effective dendritic catalyst, representing a significant shift from the expensive noble metal and platinum group metal catalysts typically employed in LOHC systems.[105] The hydrogen storage system was based on quinoxaline/1,2,3,4-tetrahydro quinoxaline utilizing water as the hydrogen source.They devised a dual-functional electrode electrocatalyst, P-WO_3/NF, achieving nearly 90% conversion in quinoxaline hydrogenation and complete conversion in dehydrogenation. The reaction conditions were characterized as mild, environmentally friendly, efficient, and safe to operate.

A novel electrochemical catalyst was designed by Kong and group for broader application of LOHCs using the electrochemical approach.[106] The catalyst Pd/Nickel foam (Pd/NF), prepared via an efficient spontaneous redox reaction, was used to study the dehydrogenation and hydrogenation of 1,2,3,4-tetra-hydro quinoxaline/quinoxaline as a hydrogen carrier. The dehydrogenation and hydrogenation reactions showed 100% dehydrogenation conversion and 95% hydrogenation conversion with 100% selectivity at room temperature and atmospheric pressure, respectively. By optimization, potentials of −0.20 V and 1.30 V were considered the most suitable for quinoline (Q) hydrogenation and 4H-quinoline (4H–Q) dehydrogenation, respectively, taking into consideration high conversion and low energy consumption. The disappearance of the oxidation peak at 1.30 V and the increase in the current density after the addition of 4H-quinoline established the involvement of Ni^{+2} in the dehydrogenation reaction.

Nie and colleagues reported a single-atom cobalt catalyst dispersed on N-doped carbon support for the acceptorless dehydrogenation and hydrogenation of N-heterocycles.[107] A series of Co-N–C(x) catalysts were prepared, thoroughly characterized, and further tested for their potential to bring about reversible hydrogen storage in certain substrates. Notably, all the catalysts exhibited dehydrogenation activity under ambient conditions, with Co–N−C (1.5) (when 1.5 mmol of 1,10-phenanthroline was used) identified as the optimal catalyst, achieving nearly 97.5% quinoline yield within 12 h. In the case of reverse hydrogenation, approximately 96% THQ yield was obtained within 9 h at 363 K and 2 MPa H_2 pressure using this catalyst. Moreover, the versatility of this catalyst was extended to other heterocyclic systems (quinolines, indoles). The study also investigated the influence of different ligand-to-metal ratios on the catalytic performance of the catalyst.

5.2.2. Bimetallic Catalysts

Kempe and group in 2016, designed a Pd_2Ru/SiCN catalyst[108] using a Ru complex and an aminopyridine palladium complex as precursors. The catalyst could hydrogenate N-ethyl carbazole (NEC) at 383 K and 20 bar H_2 pressure. The dehydrogenation on the other hand took place at 453 K with hydrogen uptake and release of 5.68 wt% and 5.51 wt%, respectively. In the same study, the authors also explored a novel hydrogen storage system derived from lignin, a rarely used biomass, which transformed it catalytically into an N-heterocyclic compound. Lignin underwent hydrogenolysis and hydrogenation to form 1,2-cyclohexanediol, which was further converted to 1,2,3,4,6,7,8,9-octahydrophenazine using an Ir@SiCN catalyst with ammonia (Figure 7a). This octahydrophenazine served as a LOHC, capable of undergoing dehydrogenation to phenazine at 463 K and reversibly reacting at 388 K and 50 bar H_2 pressure using a bimetallic Pd_2Ru@SiCN catalyst. The system exhibited a remarkable hydrogen storage capacity of 7.2 wt%, maintaining activity over seven cycles (Figure 7b). This study initiated the exploration of naturally occurring systems, modified for potential hydrogen storage, showing promising H_2 storage capabilities.

Replacing one of the precious metals with a cheaper transition metal can greatly reduce the expense of the bimetallic for industrial applications. In 2018, Chun Cai et al. explored reversible hydrogen storage of N-heterocycles under mild conditions using a MOF-immobilized Pd–Ni bimetallic catalyst, Pd–Ni@MIL-100(Fe).[43] The catalyst, benefiting from synergism and host-guest interactions showed complete dehydrogenation of 1,2,3,4-tetrahydro quinoline at 403 K and 100% hydrogenation of quinoline at 4 atm H_2 pressure. The catalytic performance of the bimetallic was attributed to the decrease in the electron density of the Pd active site because of the Lewis acidic nature of the carrier. This reduced electron density along with the synergistic interaction between Pd (ensemble effect) and Ni, which has a high affinity towards hydrogen, leads to high substrate absorbency. The catalyst also exhibited excellent reversible hydrogen storage for a range of substituted quinoline and heterocyclic derivatives.

Further studies by Beller and colleagues in 2019, showed the use of first-row intermetallic nickel silicide catalysts supported on fumed silica for dehydrogenation and hydrogenation of quinoline derivatives.[109] They synthesized three sets of catalysts with variations in ligand and pyrolysis temperature of the silica support (Table 9). Cat A comprised of an N-doped graphene-covered core ($Ni_2Si/Ni_{31}Si_{12}$) with a NiO/SiO_2 shell. Cat B is Ni-phen@SiO_2-800, while Cat C is Ni-phen@TiO_2-800. Cat A brought out reversible dehydrogenation and hydrogenation activity with dehydrogenation occurring at 473 K and hydrogenation reaction at 393 K, 50 bar H_2 affording yields of

Table 9. Catalytic dehydrogenation/hydrogenation of quinaldine/tetrahydroquinaldine using different catalysts.[109]

Catalysts	Dehydrogenation[a] H_2 Yield (%)[b]	Hydrogenation[c] Yield (%)[d]
Ni–Si/NiO-SiO_2@SiO_2 (CAT A)	74	93
Ni-phen@SiO_2–800 (CAT B)	63	92
Ni-phen@TiO_2–800 (CAT C)	53	96

[a] Dehydrogenation conditions: hydrogenated product (1.25 mmol), 300–500 mg Ni-Cat. (20 mol %), 5 mL triglyme, Ar; [b] H_2 production measured with a manual burette; [c] Hydrogenation conditions: dehydrogenated product (0.5 mmol), 40–45 mg of Ni-Cat. (4.5 mol%), 2 mL MeOH/H_2O (1 : 1), 30 bar H_2, 16 h; [d] Yields and conversions were determined by GC analysis of the liquid phase, using n-hexadecane as the internal standard.

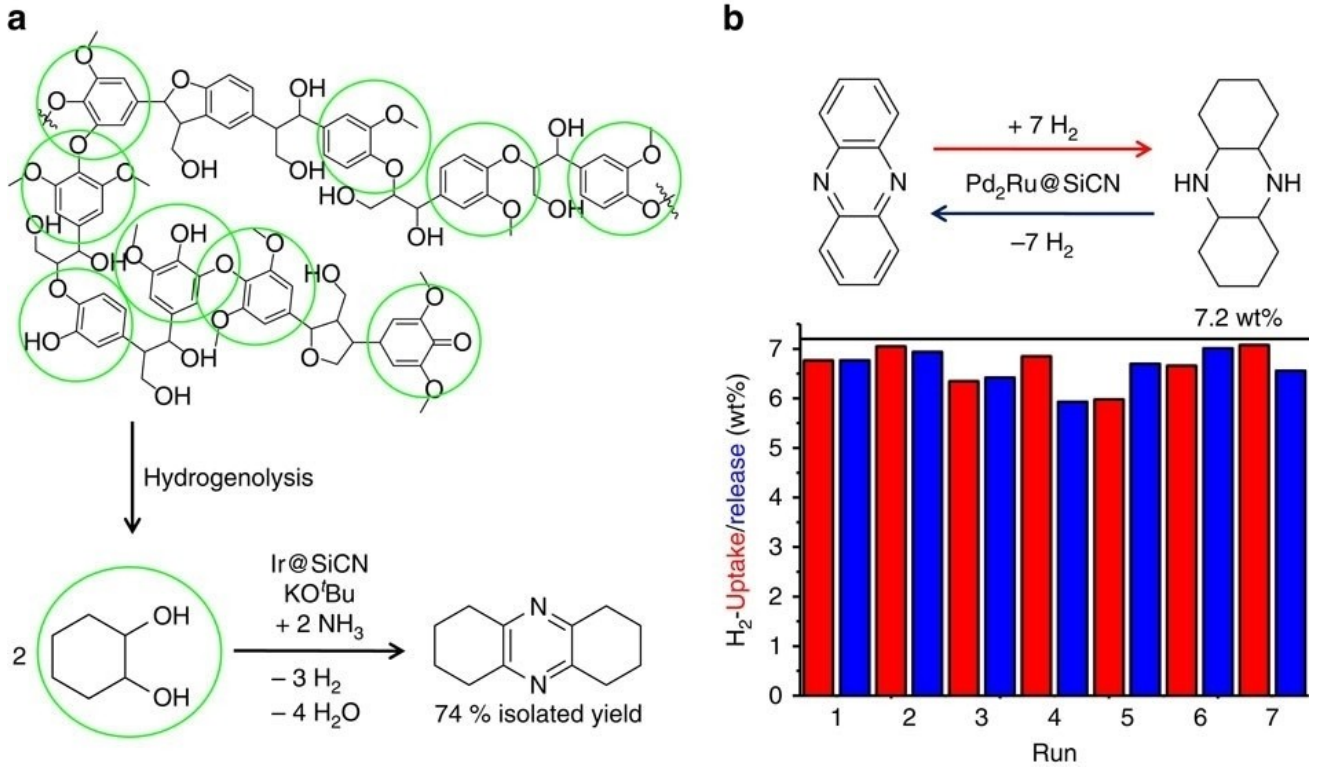

Figure 7. (a) Synthesis of octahydrophenazine from cyclohexane-1,2-diol and ammonia (b) Catalyst reusability and reversible hydrogen storage with phenazine. Reproduced under terms of the CC-BY license.[108] Copyright (2016), Daniel Forberg et al., published by Springer Nature.

93% and 100% for methyl-substituted quinoline. Table 10 summarizes the yields of the dehydrogenated and hydrogenated products of different N-heterocyclic systems using Ni–Si/NiO-SiO_2@SiO_2 (CAT A).

Furthering the scope, a range of bimetallic catalysts has been investigated, comprising combinations of two noble metals exclusively or incorporating a noble metal in conjunction with a more economical counterpart. Pd and Ru, two well-known noble metals for dehydrogenation and hydrogenation were supported on Al_2O_3 and their activities were compared with Ru–Pd bimetallic for hydrogenation and dehydrogenation studies of N-propyl carbazole/12-H–N-propyl carbazole. The studies carried out by Cheng and co-workers,[110] revealed that the hydrogenation of 4H–N-propylcarbazole (4H-NPCZ) to 8H–N-propylcarbazole (8H-NPCZ) was rapid, particularly facilitated by bimetallic catalysts due to their synergistic effects, leading to complete conversion and a hydrogen storage capacity of 5.3 wt%. The bimetallic catalyst exhibited the highest catalytic conversions compared to the monometallic Pd/Al_2O_3 and Ru/Al_2O_3 catalysts. In contrast, the sequential dehydrogenation process from 12H-NPCZ to NPCZ involved intermediates such as 8H-NPCZ and 4H-NPCZ, with the rate-determining step being the conversion from 4H-NPCZ to NPCZ. The catalyst was also found to be stable over three cycles of cyclic dehydrogenation-hydrogenation.

In 2020, Dyson and colleagues investigated another bimetallic catalyst, PdAu, for acceptorless dehydrogenation and hydrogenation of heterocycles, amines, and alcohols.[111] Supported on multiwalled carbon nanotubes with preferentially exposed Pd_3Au_1(111) facets, the catalyst was synthesized via a reduction method employing trisodium citrate dihydrate as a stabilizing agent. The bimetallic catalyst demonstrated high catalytic activity yielding nearly 96% and 95% conversion for dehydrogenation and hydrogenation of quinolines, respectively. Furthermore, it displayed good catalytic activity across a range of N-alkylated amines and other heterocycle derivatives. The

Table 10. Catalytic dehydrogenation/hydrogenation of different N-heterocyclic systems using Ni–Si/NiO-SiO_2@SiO_2 (CAT A) catalysts.[109]

Catalysts	N-heterocyclic system	Dehydrogenation: H_2 Yield (%)[a]	Hydrogenation: Yield (%)[b]
Ni–Si/NiO-SiO_2@SiO_2 (CAT A)	2-methyl quinoline	74	93
	Quinoline	57	91
	7-methyl quinoline	62	92

[a] Dehydrogenation: Hydrogenated product (1.25 mmol), 500 mg of Cat. A (20 mol%), 473 K, 24 h. 5 mL triglyme, Ar.; [b] Hydrogenation: Dehydrogenated product (0.25 mmol), 100 mg of Cat. A (20 mol%), 2 mL triglyme, 393 K, 50 bar H_2, 16 h.

reaction mechanism for the dehydrogenation and hydrogenation of heterocyclic compounds using the Pd_3Au catalyst is shown in figure 8A. The superior performance of the $Pd_3Au_1(111)$ surface was attributed to its lower energy barriers for the dehydrogenation and hydrogenation steps compared to the Pd (111) facet (Figures 8B and C).

The 12H–N-ethylcarbazole/N-ethylcarbazole (12H-NEC/NEC) system is one of the systems that has been studied in great detail for reversible hydrogen storage owing to its high hydrogen content of 5.8 wt%. The dehydrogenation rate of NEC is faster than dodecahydrocarbazole because of the presence of the ethyl group preventing strong binding of the molecule to the catalyst surface. In their recent 2021 study, Li and colleagues investigated the synergistic effects of a noble metal-free catalyst, Co–B/Al_2O_3-YH_{3-x}, comprising alumina-supported cobalt boride with non-stoichiometric yttrium trihydride species.[112] This catalyst was utilized for the reversible dehydrogenation and hydrogenation of the 12H-NEC/NEC system, a promising LOHC with generally sluggish kinetics, showing excellent activity. The dehydrogenation process takes place at 473 K, 0.1 MPa H_2 while the hydrogenation process, at 453 K, 10 MPA H_2 with interconversion being more than 94% and demonstrating excellent recyclability. The catalyst's enhanced performance was attributed to synergistic interactions between Co–B and YH_{3-x}. The calculated activation energies for hydrogenation and dehydrogenation are 149 ± 1 kJ mol^{-1} and 199 ± 7 kJ mol^{-1}, respectively. The YH_{3-x} species seem to play a crucial role in the hydrogen transfer pathway, facilitating rapid hydrogen absorption-desorption kinetics, while Co–B activates the NEC-12H-NEC. The non-stoichiometric YH_{3-x} featured both lattice hydrogen and hydrogen vacancies, aiding in reversible hydrogen transfer.

Sun et al.[41] evaluated the role of different supports Al_2O_3, SiO_2, TiO_2, C, and MCM-41 loaded with Pd, Rh, Ir, and Ru nanoparticles for dehydrogenation and hydrogenation reactions. Their study established alumina to be the most efficient among the different supports, and the Pd/Al_2O_3 catalyst and Rh/Al_2O_3 catalyst demonstrated excellent results for dehydrogenation and hydrogenation reactions, respectively. The bimetallic system Pd–Rh/Al_2O_3 was therefore tested for reversible hydrogen storage in 12H–N-ethylcarbazole/N-ethylcarbazole (12H-NEC/NEC) system showing a hydrogen release capacity of 5.48 wt% and an uptake of 5.43 wt%. The DFT calculations, energy profiles, and adsorption energies also demonstrated that the hydrogenation process on the surface of the Pd_6/Al_2O_3 catalyst is all endothermic with values of 0.033, 1.388,1.514 and 0.939 eV for the step-wise hydrogenation of NEC (NEC-4H-NEC-8H-NEC-12H-NEC). On the other hand, the reaction energies for the stepwise hydrogenation process using the Rh_6/Al_2O_3 catalyst were −1.037, −0.228, −0.021, and −1.197 eV suggesting that hydrogenation is thermodynamically favorable on the Rh surface. In the case of the bimetallic system, the hydrogenation

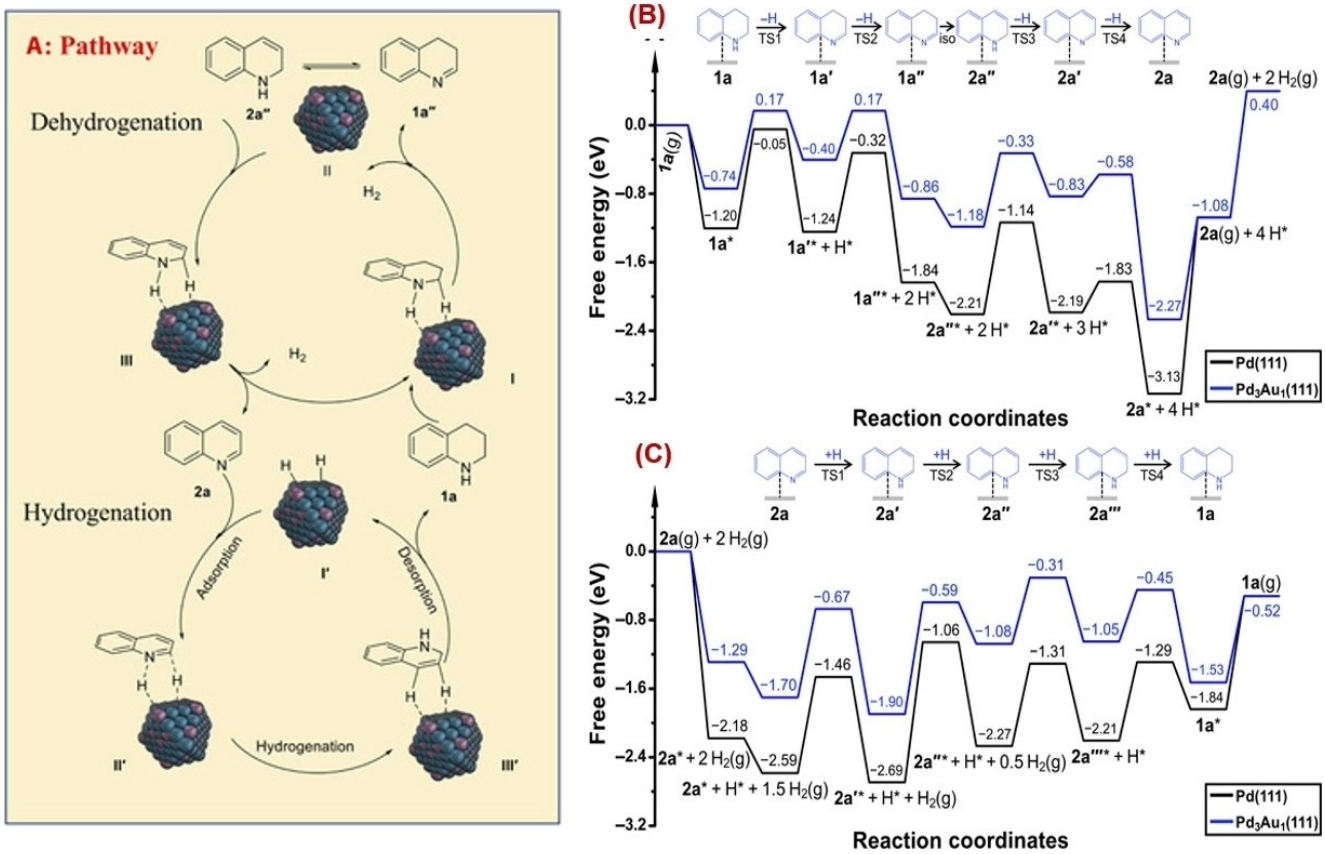

Figure 8. (A) Proposed mechanism of the dehydrogenation and hydrogenation cycles; (B) Dehydrogenation at 413 K and (C) hydrogenation at 353 K on the Pd(111) and $Pd_3Au_1(111)$ surfaces. Adapted under terms of the CC-BY-NC license.[111] Copyright (2020), Xinjiang Cui et al., published by Science (AAAS).

process from NEC to 4H-NEC and from 6H-NEC to 8H-NEC on the (110) plane of Pd_4Rh_2/Al_2O_3 is exothermic by −1.366 and −1.356, respectively. The reverse dehydrogenation from 12H-NEC to 8H-NEC and 6H-NEC to 4H-NEC, on the other hand, is endothermic, indicating a synergistic interaction between the Pd and Rh nanoclusters

Zheng and colleagues presented a $LaNi_{5+x}$ $(0<x<1)$ catalyst featuring a distinctive core-shell structure for reversible hydrogen storage in NEC/12 H-NEC.[113] Obtained via a CaH_2 reduction method in KCl molten salt, the catalyst is comprised of a La oxide amorphous layer enveloping Ni nanocrystals, with $LaNi_5$ forming the core. A sufficient number of H-bonding sites were provided by the catalyst with $LaNi_5$ acting as a dominant host for atomic H. This catalyst was found to be active for up to 9 dehydrogenation-hydrogenation cycles, with Ni nanocrystals providing adsorption and activation sites for NEC/12 H-NEC, while the $LaNi_5$ core furnishes H-bonding sites. The unique Ni/$LaNi_5$ interface facilitates H-transfer to and from the activated NEC/12 H-NEC. Pressure also plays an important role in driving the migration of hydrogen atoms in opposite directions. During the hydrogenation process, high pressure of H_2 leads to the formation of $LaNi_5$-H solid solution, from which H is transported to the $LaNi_5$/Ni interface, further migrates on the Ni surface, and finally hydrogenates the unsaturated heterocycle (Figure 9). The same pathway is followed for the dehydrogenation, which occurs at lower pressure. Hydrogen from the substrate migrates over the Ni surface to the $LaNi_5$/Ni interface and is finally released as H_2. With a reversible hydrogen storage capacity exceeding 5.5 wt% below 473 K, the catalyst maintains stability throughout multiple cycles.

In their study, Yang and colleagues investigated the $Ru_{2.5}$-$Pd_{2.5}$ bimetallic system's potential for reversible hydrogen storage using N-heterocycles.[114] They observed that the hydrogenation process proceeded gradually, involving the saturation of double bonds within the system. The bimetallic catalyst was prepared by reduction with an Ar-H_2 gas mixture, resulting in the formation of small-sized nanoparticles that exhibited excellent dispersion without agglomeration. This enhanced dispersion along with the synergistic effect, contributed to improved catalytic performance, achieving complete transformation in just 40 min. Despite exhibiting good cyclic hydrogenation ability, the catalyst was found to undergo degradation during the dehydrogenation cycle. In the initial cycle, the hydrogen storage and release capacities were found to be 5.41 wt% and 5.43 wt%, respectively. However, by the fifth cycle, these values decreased to 4.90 wt% and 5.24 wt%, indicating some loss in performance over repeated cycles.

Chen's group developed a Rh–Co/γ-alumina bimetallic catalyst for reversible (de)hydrogenation of NEC with a 5.8 wt% hydrogen storage capacity.[115] The catalyst outperformed the monometallic analogs due to synergistic effects, effecting 68.28% H_2 release at 453 K and 93.6% uptake at 403 K. Based on computational studies, it was concluded that the introduction of Rh to Co balanced the metal-H interaction and reactants-intermediate interaction favoring the hydrogenation of NEC. From the adsorption energy values (Table 11), it could be deciphered that the dehydrogenation process of 12H-NEC is significantly hindered by the strong interaction between hydrogen and cobalt, causing its slowdown on Co(111). Introducing rhodium alongside cobalt resulted in a more balanced interaction with hydrogen, thereby facilitating the dehydrogenation reaction. The bimetallic Rh_1Co catalyst achieved a synergistic balance between different interactions on their surface compared to their monometallic analogs, ultimately improving overall catalytic performance.

Chung and collaborators investigated the reversible dehydrogenation/hydrogenation of the quinoline system using a bimetallic Co/Zn catalyst loaded on nitrogen-doped carbon, denoted as Co_xZn_y-NC.[116] Their study revealed that the catalyst brought out three consecutive cycles of hydrogen storage/release. Through a series of control experiments, the significance of free N–H groups/N-atoms for facilitating the dehydrogenation/hydrogenation reactions was highlighted. The first step of the dehydrogenation and the hydrogenation reaction mechanism involves binding of the substrate to the Co-active site via nitrogen. The first release of H_2 during the dehydrogenation step is from the N–H bond and the adjacent C–H bond, following which there is isomerization of the double bond in the ring to the other position, with the removal of the second H_2 molecule from the same N–H and C–H bond (Scheme 2A), and the process continues. A similar mechanism is followed during the hydrogenation processes, where the C=N bond of the substrate gets hydrogenated, followed by isomerization of the double bond and subsequent hydrogenation of the C=N bond. (Scheme 2B). The same LOHC system was also explored using catalysts prepared by the electrostatic adsorption method.[117] The NPs prepared by this method have an average particle size of 3.88 nm and are highly dispersible in solvents. In a recent novel work,[117] Bai and co-workers synthesized PdRu/SBA-15 catalyst by a glow discharge plasma reduction of double

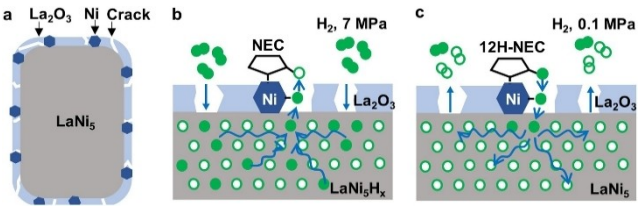

Figure 9. (a) Structure illustration of a LaNi5.5 nanoparticle. The H transfer processes in (b) NEC hydrogenation and (c) 12 H-NEC dehydrogenation. Reproduced from Ref. [113] Copyright (2021) with permission from Elsevier.

Table 11. Adsorption energy values (kJ mol^{-1}) of substrates and intermediates on the (111) facet of Co, Rh, and Rh_1Co.[115]

	Co (111)	Rh (111)	Rh_1Co (111)
H	−292.8	−268.7	−288.7
NEC	−113.6	181.9	−102.8
4H-NEC	−99.5	−147.2	−89.3
6H-NEC	−99.0	−132.3	−112.0
8H-NEC	−40.3	−63.1	−44.6
12H-NEC	−65.9	79.9	64.2

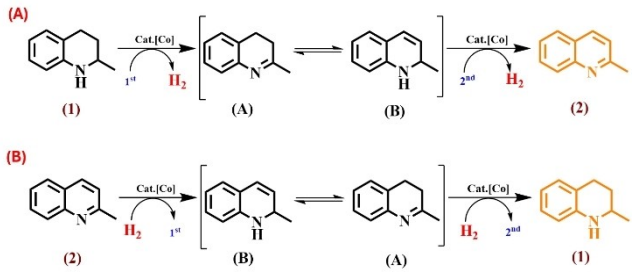

Scheme 2. Schematic showing the dehydrogenation and hydrogenation mechanistic pathway for methyl quinoline. Adapted from Ref. [116] Copyright (2023) with permission from Elsevier.

complex salt on SBA-15. The Ru cation precursor interacts with the support via electrostatic adsorption followed by phase transfer of the Pd anion with the help of quaternary ammonium cation, on Ru forming the PdRu/SBA-15. The LOHC chosen for their study was the 12H-NEC/NEC system which undergoes hydrogenation up to 99.8% at 373 K and 5 MPa and exhibits almost 100% efficiency for dehydrogenation at 453 K.

Liu et al. also addressed the need for a single catalyst capable of dehydrogenation and hydrogenation by studying the Ni/Pd-loaded alumina catalyst.[118] The addition of Pd shifted the d-band center of Ni towards the Fermi level and also brought about a change in the electronics around Ni (supported by DFT) thereby enhancing the adsorption and hence the activity of the catalyst. The binding of H* on $Pd_1Ni(111)$ is lower, $-224.6\ kJ\,mol^{-1}$ compared to adsorption on Ni(111), $-287.5\ kJ\,mol^{-1}$. This is due to the addition of Pd to Ni, which enhances the adsorption of dehydrogenation products, resulting in enhanced dehydrogenation on the bimetallic surface. The hydrogenation reaction takes place at 60 bar pressure and 433 K for 1 h, while for the reverse reaction, a temperature of 453 K was employed. The bimetallic catalyst exhibited 25-fold higher dehydrogenation and 20-fold higher hydrogenation activity compared to standard monometallic catalyst.

5.3. Circular Liquid Hydrogen Carriers

Prato and co-workers in 2017 designed a ternary hybrid catalyst integrating Pd nanoparticles of roughly 1.5 nm on an oxidized Single-Walled Carbon NanoHorns (ox-SWCNHs) followed by stabilization with a TiO_2 outer shell.[119] They utilized the catalyst for the circular hydrogen consumption/release cycle of the CO_2/formic acid couple where CO_2 acts as an organo-catalytic mediator. The reaction occurs in series with the reduction of CO_2 to HCOOH followed by the decomposition of HCOOH to H_2. They, through a series of experiments, demonstrated that the synergistic effects of all the three components in the catalyst are necessary for their excellent performance in the electrocatalytic reduction of CO_2 at a low overpotential regime.

In 2018, Chen and co-workers employed a citrate-complex method for the preparation of Cu–Zn–Zr–Al–O catalysts and studied the dehydrogenation of ethanol to ethyl acetate and the reverse hydrogenation of ethyl acetate to ethanol.[120] The synthesis of the quaternary catalyst was carried out in water, ethanol, and ethyl acetate as solvents. The solvents chosen for the synthesis seemed to influence the activity of the catalyst. The use of solvents with low dielectric constant like ethanol, accelerated the complexation process between the metal nitrates and citric acid, leading to the formation of well-dispersed small copper nanoparticles (8–10 nm). These nanoparticles interacted strongly with M_xO_y, compared to those prepared using high dielectric constant solvents where heterogeneously distributed agglomerated structures were formed, showing the important role played by the solute-solvent interaction. The dehydrogenation of ethanol was performed at 493 K, and 0.1 MPa with liquid hourly space velocity (LHSV) of $0.4\ mLgcat^{-1}\,h^{-1}$, resulting in 78.9 wt% conversions of EtOH. The hydrogenation reaction of ethyl acetate took place at 513 K and 2.4 MPa resulting in 95.8% conversion using the Cu–Zn–Zr–Al–O/ethanol catalyst. Both the reactions resulted in the formation of side products.

In 2014, Won Yoon and colleagues explored carbon dioxide-mediated reversible hydrogen storage using Pd nanoparticles (average size of 1.7 nm) supported on mesoporous carbon nitride ($Pd/mpg\text{-}C_3N_4$) without any stabilizing ligands, preventing agglomeration.[121] The high dispersity of the Pd nanoparticles was attributed to the interaction between the N atoms in the support and the cationic Pd^{2+} ions. The synergy between the metal and the support was crucial, with the Pd nanoparticles serving as the active catalytic sites while the N atoms promoted the deprotonation step, further improving the dehydrogenation performance. The dehydrogenation reaction was conducted under ambient conditions, achieving a TOF of $144\ h^{-1}$, comparable to the highest TOF reported for base-free dehydrogenation of formic acid. Additionally, the catalyst was tested for hydrogenation, successfully producing formic acid through the hydrogenation of carbon dioxide.

In the same year, Yamashita proposed a synthesis method for a PdAg bimetallic system supported on phenylamine-functionalized mesoporous carbon, aiming to demonstrate reversible dehydrogenation-hydrogenation using the formic acid/CO_2 system.[122] The catalyst exhibited outstanding activity, with a TOF of $5638\ h^{-1}$ for dehydrogenation and a TON of 839 for hydrogenation, which was attributed to a combination of synergism and amine functionalization. The functionalization of the supports not only enhanced both dehydrogenation and hydrogenation reaction rates but also modified the electronic state of Pd and increased the adsorption capacity of CO_2. To elucidate the role of amine functionalization in the catalyst's high activity, energy profile studies were carried out (Figures 10 and 11). These calculations suggested that formic acid forms an acid-base pair with phenylamine on the Pd–Ag catalyst, which results in the spontaneous generation of $HCOO^-$. The HCOOH interacts with the PdAg catalyst via its carbonyl oxygen and non-carbonyl oxygen, this interaction leads to the elongation of the O–H bond. In the hydrogenation step, phenylamine stabilized the intermediate formed through a N–H···O interaction, contributing to the catalyst's enhanced performance. They also studied another PdAg/SBA-15 catalytic system for the reversible dehydrogenation and hydrogenation of formic acid

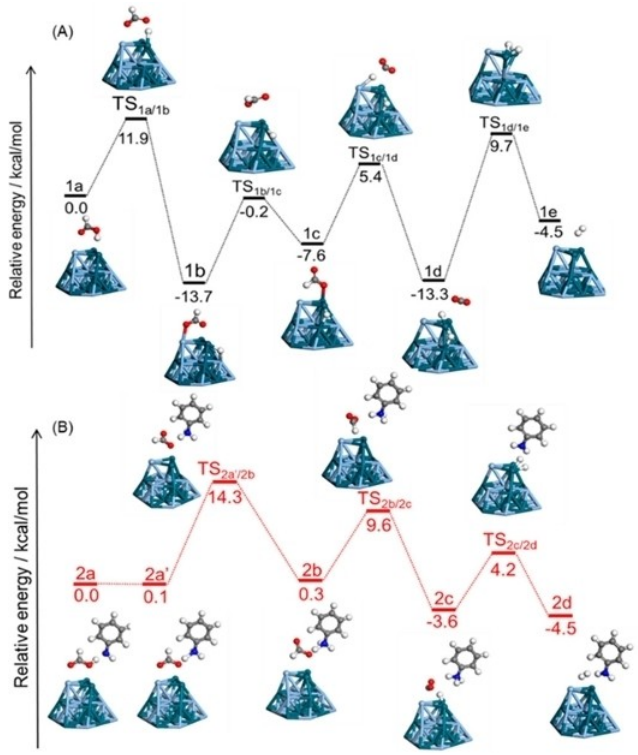

Figure 10. Potential energy profiles for the dehydrogenation of CO_2 in the (A) absence and (B) presence of phenylamine. Reprinted with permission from Ref. [122]. Copyright {2018} American Chemical Society.

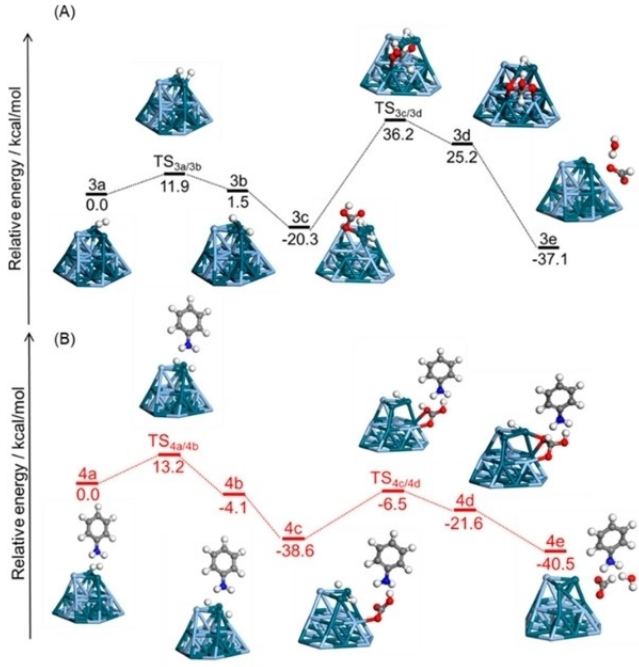

Figure 11. Potential energy profiles for the hydrogenation of CO_2 in the (A) absence and (B) presence of phenylamine. Reprinted with permission from Ref. [122]. Copyright {2018} American Chemical Society.

and CO_2.[123] The catalyst demonstrated excellent activity due to the high dispersion and amine functionalization of the mesoporous carbon. Using both experimental and DFT calculations, the authors established the role of weakly basic amine functionality on the adsorption and stabilization of formic acid and CO_2 through cooperative action. The incoming HCOOH interacts with the amine group on SBA-15 forming an acid-base pair. The HCOOH then interacts with the Pd catalyst surface via the carbonyl oxygen atom and hydrogen atom at the carbon. This interaction led to the elongation of the O–H bond. The next step was the C–H bond cleavage leading to CO_2 formation (Figure 10). The CO_2 hydrogenation on the other hand started with H_2 dissociation, followed by the insertion of CO_2 to form a formate intermediate, and finally formic acid and its desorption (Figure 11). They found that the role of amine was not only the stabilization of the intermediate but also its relatively lower basicity led to a concentration effect on the surface of the catalyst and thereby enhancing the catalytic activity.

Yan and colleagues in 2020 explored reversible hydrogen storage in the HCOOH/CO_2 system using nanoclusters encapsulated in silicalite zeolite (PdMn@S-1) under in situ hydrothermal conditions.[124] DFT calculations showed that adding Mn enhanced the catalytic activity by favoring a compact structure formation, preventing strong interaction of the intermediates with the Pd active sites, and improving the activity of Pd. In addition, it facilitates the formation of bicarbonate species during the hydrogenation of CO_2 and further accelerates the hydrogenation of these bicarbonates to formates on the Pd surface.

As discussed previously, the use of molecular organometallic catalysts for dehydrogenation has garnered significant interest, particularly for their ability to operate under mild reaction conditions. Various factors including the nature of the linker,[72,125–127] the metal center, the backbone of the pincer, and the co-ligands affect the electronic and steric properties of these catalysts. While numerous studies have explored the reversible dehydrogenation and hydrogenation of LOHCs using pincer complexes, most have focused on homogeneous catalysts.[64–65,74,45] Reports on the heterogenization of pincer complexes onto solid supports for dual dehydrogenation and hydrogenation applications are limited. Notably, one study highlights the heterogenization of an iridium pincer complex for the isopropanol/acetone system. Wendt and colleagues effectively integrated the high selectivity and reactivity of iridium complexes with the benefits of a heterogeneous catalyst for isopropanol dehydrogenation in a continuous-flow reactor.[128]

Isopropanol, recognized as a non-toxic and safe substrate, has emerged as a promising LOHC. The authors synthesized an iridium pincer complex, [(2,6-(^{t}Bu$_2$PO)$_2$C$_6$H$_3$)IrHCl], and successfully immobilized it on a silica support. The resulting catalyst was then evaluated for acceptorless dehydrogenation of isopropanol in a continuous-flow setup, achieving remarkable TONs of up to 1,600,000 and TOFs as high as 160,000 h^{-1}. This study paves the way for innovative applications in reversible hydrogen storage using organometallic complexes.

In 2022, an organometallic heterogeneous catalyst was studied by Macchioni and the group for the hydrogenation and dehydrogenation of CO_2 and formic acid, respectively (Scheme 3).[49] The catalyst Ir_PicaSi_SiO_2 (PicaSi: picolinamide

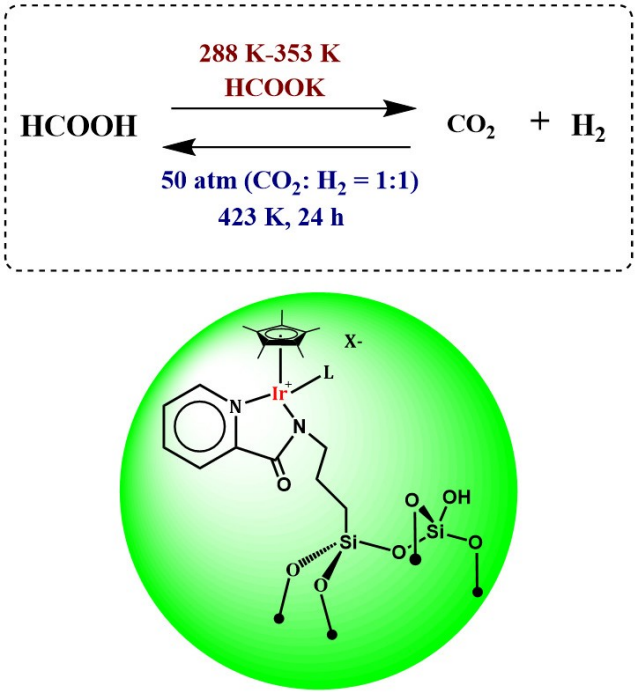

Scheme 3. Reversible dehydrogenation-hydrogenation of the HCOOH/CO_2 system using the Ir_PicaSi_SiO_2 catalyst.[49]

ligand having a (3-triethoxysilyl)propyl group on the nitrogen atom of the amide moiety) was obtained in two steps. First, the (3-triethoxysilyl)propyl fragment was supported on mesoporous silica via a sol-gel process to obtain PicaSi_SiO_2. Next, a complexation process followed, involving the PicaSi_SiO_2 with iridium organometallic moiety, $[Cp^*IrCl_2]_2$. The highest TOF of 636 h^{-1} was realized at pH 3.7. The hydrogenation was carried out under batch conditions at 423 K and 50 atm (CO_2:H_2 = 1:1), with a TON of 6983 with Ir content being 0.057 mmol.

Sooknoi and co-workers studied another novel hydrogen storage material, 3-acetyl pyridine (AcP) modified with MIL-101(Cr).[129] The Pd nanoparticles are encapsulated in the AcP-grafted MIL-1010(Cr) to drive the dehydrogenation-hydrogenation reactions. The interaction between the Cr^{+3} in MIL-1010(Cr) and AcP via coordinative covalent bonding with the N-pyridine ring of AcP increased the stability of the AcP-MIL-101(Cr). This interaction between the Pd and MOFs prevented the agglomeration of Pd. The hydrogenation and the dehydrogenation cycles proceeded with a simple change in the partial pressure of the system at elevated temperatures. The authors also found that the operating temperature played a role in the dehydrogenation/hydrogenation cycle. The hydrogenation at the carbonyl group of AcP gave 3-(1-hydroxyethyl)pyridine (HEP) whereas the dehydrogenation step regenerated the carbonyl AcP. Even though the hydrogen storage capacity of the new carrier was not impressive, (< 0.1 wt%), the system was unique because it could be operated at constant temperature and pressure by simply tuning the partial pressure of hydrogen.

6. Summary and Outlook

The transformation that we need today is the transition towards a hydrogen economy. This transition holds immense promise for a sustainable future with Liquid Organic Hydrogen Carriers (LOHCs) emerging as a pivotal concept. However, realizing this potential involves overcoming numerous challenges, particularly in the catalyst design and infrastructure development. Different LOHC systems have been studied in the last few decades and this review offered a comprehensive look at the recent developments in reversible hydrogen storage. The first step to this transition is the quest for a suitable catalyst capable of facilitating reversible dehydrogenation/hydrogenation reactions under mild conditions, ensuring efficiency and stability. Recent efforts have been focused on hybrid heterogeneous catalysts, exploring monometallic, bimetallic, and pincer complexes supported on various substrates. Incorporating a second metal has shown potential in enhancing storage capacities, because of the synergistic effects between the two metals. Yet, technical limitations persist, particularly in developing effective and stable dehydrogenation catalysts that are resistant to deactivation. The next step, finding an LOHC system suitable for reversible dehydrogenation and hydrogenation under mild conditions remains a priority. The cyclic hydrocarbons have been extensively studied and tipped as potential LOHC systems with practical applications. Different strategies such as substituting aromatic rings or increasing the number of cyclic rings to lower the dehydrogenation enthalpy have been explored, albeit with limitations like solidification at room temperature. Similarly, replacing carbon atoms with heteroatoms offers promise but often at the expense of hydrogen storage capacity. Challenges also arise with certain LOHCs, such as formic acid and alcohols, necessitating CO_2 capture for material regeneration. Table 12 summarizes the various heterogeneous catalysts covered in this review, including the conditions for dehydrogenation and hydrogenation reactions.

The compatibility of LOHCs with the existing infrastructure, similar to crude oil, facilitates a seamless transition in the industrial and automotive sectors, promoting a carbon-free economy. Other factors must also be considered when selecting LOHCs as alternative energy systems, including affordability, energy density, safety, and environmental impact. Compared to other technologies that are available for long-distance hydrogen fuel import/export, the existing global infrastructure is compatible with the transportation and storage of liquid hydrocarbons. However, the widespread adoption of LOHC technology necessitates additional infrastructure for storage and handling. There is significant potential for advancing catalyst design to improve the dehydrogenation and hydrogenation processes within LOHC systems.[5,12,21] Enhancing overall activity, selectivity, and performance through innovative cost-effective catalysts is crucial for the economic viability of LOHC technologies. Another key area for improvement is the modification and installation of infrastructure to ensure the safe distribution of LOHCs. Effective global implementation will also necessitate the design of suitable reactors tailored for LOHC applications. However, challenges persist regarding the man-

Table 12. Different heterogeneous catalysts studied for the reversible dehydrogenation-hydrogenation reactions.

LOHC systems	Catalysts	Dehydrogenation conditions	Hydrogenation conditions	Comments on reactivity and stability
Terphenyl/tercyclohexane	M/SiO_2, M/Al_2O_3, M/C, M/Sibunit, (M=Pd, Pt)[76–78] 3 wt% Pt/C (Sibunit)	100 mg catalyst, 400 mg TCH, Substrate/catalyst ratio = 4; 583 K – 623 K, Stir 533 K - 613 K, 1 bar pressure, LHSV = 1 h^{-1} Catalyst 6 cm^3, Substarte, feed flow rate 6 mL h^{-1}	80 mg catalyst, 800 mg TPh, Substrate/catalyst ration = 10; 50 atm hydrogen, 433 K, 2 h, Stir Substrate/catalyst ratio 10; 70 bar pressure, 453 K	10% Pt/C: Hydrogenation rates 24.6 l/g-Cat·h. Dehydrogenation rate: 12.0 l/g-Cat·h.; Dh: 91% conversion; Hy: 99% conversion; Stable up to 2 cycles.
Terphenyl/perhydroterphenyl	1% Pt/Mg_2NiH_x[79]	Catalyst 1 g, 593 K,15 cc of substrate	413 K, H_2 pressure 50–60 atm	Dh: rate of hydrogen release 26 mL/min Hy: Hydrogen storage capacity 7.25 wt%; Stable up to 20 cycles of hydrogenation.
Methylcyclohexane/toluene	1.0 wt% Pt/zeolite beta catalyst[29]	1 atm H_2 pressure, 633 K, 6.22x10^4 s g-cat/mol MCH	8 bar H_2 pressure, 536 K, H_2/Tol molar ratio 4.34 (Equilibrium reached)	Dh: ~80% conversion at 633 K, H_2/MCH molar ratio 4.21, P = 1.013 bar; Hy: ~100% conversion at 6 bar, H_2/MCH molar ratio 4.34, T = 493 K.
Cyclohexane/benzene	Pt@TiO_2 NPs[80]	10 mg catalyst, P < 1 Pa, 100 μmol of cyclohexane, RT, 300 W Xe lamp	10 mg catalyst, P < 1 Pa, 300 μmol of H_2, 100 μmol of benzene, RT, 300 W Xe lamp	Dh: TON 40; TOF 20 h^{-1}; Hy: TON 38.8; TOF 38.8 h^{-1} at 323 K.
H18-Dibenzyltoluene/dibenzyltoluene	Pt/Al_2O_3[81]	0.015 mol% Pt (0.3 wt% Pt/Al_2O_3), 300 g H0-DBT, 564 K, 1.05 bar hydrogen pressure, 20 h	574 K, 30 bar hydrogen pressure, 4 h	The degree of hydrogenation > 0.95 in all cycles and the degree of hydrogenation during dehydrogenation sequences < 0.3; Stability tested up to four cycles of reversible hydrogen storage.
H18-Dibenzyltoluene/dibenzyltoluene	5 wt% Pt/Al_2O_3[31]	543 K, 300 min, 1 atm pressure, Catalyst: Substrate 0.3%;	413 K, H_2 pressure 4 MPa, 35 min	Dehydrogenation 56.3% after 300 min and complete hydrogenation in 35 min; Stability tested up to five cycles of reversible hydrogen storage.
H18-Dibenzyltoluene/dibenzyltoluene	3 wt% Pt/Al_2O_3[82]	543 K, atmospheric pressure.	10 g DBT, 0.3 mol% catalyst, 413 K, 4 MPa H_2 pressure.	3% Pt/Al_2O_3: Dh: Degree of dehydrogenation 71.7%; TOF ~4 s^{-1}; Hy: Degree of hydrogenation 100%; Stability tested up to four cycles of reversible hydrogen storage.
Polycyclic aromatic hydrocarbons	3 wt% Pt/C[83]	533 K–613 K and volume hourly space velocity 1 h^{-1}.	Catalyst: Substrate volume ratio 1:10, 453 K–553 K, 70–90 atm H_2 bar pressure,	Decalin/Naphthalene system: Dh: > 96%; Hy: Hydrogenation rate 1116.6 mol/g(Pt)*h^{-1} (*10^{-2}); Activation energy 10.3 kJ/mol – 143.8 kJ/mol.
Cyclohexane/benzene (vapor phase)	Nano-Pd/CeO_2[84]	573 K – 773 K, feed gas consisting of cyclohexane	50 mg of catalyst, 373 K – 473 K with feed gas consisting of benzene and H_2 (1:30) with a flow rate of 1 0 mL/min	Dh: 65.3% conversion with 100% selectivity; Hy: > 99% conversion with 100% selectivity; TOF at 373 K, 2.78x10^{-2} s^{-1}; H_2 production capacity of 73.77 g/h.
Cyclohexane/benzene Methylcyclohexane/toluene	Pt_1/CeO_2[27]	100 mg catalyst, Gas flow: N_2 30 ml/min; Cyclohexane or MCH feeding rate 3 mL/h, 623 K	40 mg catalyst, n-heptane, 27.22 atm H_2 at 393 K, 8–12 h.	TOF of hydrogen production 29300–32000 mol_{H2} mol_{Pt}^{-1} h^{-1} for methylcyclohexane and cyclohexane; TON for hydrogenation 800/$mol_{toluene}$ mol_{Pt}^{-1}–1700/$mol_{benzene}$ mol_{Pt}^{-1}; Stability tested up to four cycles of reversible hydrogen storage.
Cyclohexane/benzene (vapor phase)	1.0 wt% Pd/γ-alumina[28]	473 K – 723 K, atmospheric pressure, feed gas consisting of cyclohexane	50 mg of catalyst, 373 K - 473 K, atmospheric pressure with feed gas consisting of benzene and H_2	Dh: 90.94% conversion at 673 K; Hy: 97.51% conversion with 100% selectivity using 1PAN15

Table 12. continued

LOHC systems	Catalysts	Dehydrogenation conditions	Hydrogenation conditions	Comments on reactivity and stability
		feed gas space velocity of 14,400 $mL h^{-1} g cat^{-1}$	(1:30) with feed gas space velocity of 14,400 $mL h^{-1} g cat^{-1}$	catalyst; Hydrogen storage capacity of 1PAN15 catalyst reached 6.54 wt% (Theoretical value 7.19 wt%).
Methylcyclohexane/ toluene	Cu–Pt/S-1[89]	15 ml min^{-1} H_2 stream, 623 K, 0.1 MPa, and 4.6 h^{-1} MCH weight hourly space velocity (WHSV)	Cyclohexane, 1.5 MPa [$n(H_2)/n$-(toluene) ~3.1], 423 K, 300 rpm	Dh: H_2 release rate 445.3 mmol g_{Pt}^{-1} min^{-1} with 92.26% conversion; Hy: Hydrogen storage rate 1271 mmol g_{Pt}^{-1} min^{-1} with >99.9% conversion; Stability tested up to four cycles of reversible hydrogen storage.
Cyclooctane/Cyclooctene	Pd–Ru/Ir/Al_2O_3[90]	443 K, Ar, atmospheric pressure	298 K, 1 atm H_2 pressure	Dh: TON 571; TOF 95.2 h^{-1}; Hy: TON 300; TOF 150 h^{-1}; Stability tested up to two cycles of reversible hydrogen storage.
1,2,3,4-tetrahydroquinoline/quinoline	Cu/TiO_2[91]	0.5 mmol substrate, Cu catalysts (0.1 mmol), mesitylene, 423 K, Ar flow, 16 h	0.5 mmol substrate, Cu catalysts (0.1 mmol), mesitylene, 5 atm H_2, 423 K, 3 h or 1 atm H_2, 6 h	Dh: >99% conversion and >99% yield; Hy: >95%conversion and 95% yield; TON ~5 for both dehydrogenation and hydrogenation; Stability tested up to two cycles of reversible hydrogen storage.
Quinoline and other heterocyclic derivatives	Pt NW[92]	1 mmol THQ, 0.005 mmol, methanol, 313 K, 1 bar O_2 bar	1 mmol Quinoline, 0.005 mmol catalyst, methanol,1 bar H_2 pressure, 353 K, 24 h	Quinoline/1,2,3,4-tetrahydro quinoline Dh: >99% yield; TON 198; Hy: 92.1% yield; TON 183; Stability tested up to 10 cycles of reversible hydrogen storage.
1,2,3,4-tetrahydroquinoline/quinoline	Co@NGS[93]	1 mmol THQ, 2.5 mol% catalyst, n-dodecane, methanol, 0.1 MPa, 353 K, O_2, 6 h	0.5 mmol quinoline, Isopropanol, n-dodecane,10 mol% catalysts, 4 MPa, 413 K	Co@NGS-800: Dh: 90% conversion with 98% selectivity and rate of 0.36 mol L^{-1} h^{-1}; TON 36 for 6 h; Hy: 84% conversion with 98% selectivity and rate of 0.024 mol L^{-1} h^{-1}; TON 8.4; Stability tested up to 12 cycles of hydrogenation and 6 cycles of dehydrogenation.
2-methyl-1,2,3,4-tetrahydroquinoiline/2-methyl quinoline and other heterocyclic derivatives	MNPs/SBA-15 (M=Pd, Pt, Rh)[94]	0.1 mmol reactant, 2.5 mol% catalyst, Toluene, 403 K, 23 h	0.1 mmol reactant, 2.5 mol% catalyst, 333 K, 1 atm H_2, 24 h	2-methyl quinoline, using PtNPs/SBA; Dh: TON 40; TOF 1.7 h^{-1}; Hy: TON 40; TOF 1.7 h^{-1}; No change in particle size after recyclability.
1,2,3,4-tetrahydroquinoline/quinoline	5 wt% Pt/C[95]	o-xylene, n-dodecane, 0.1 mol% catalyst, reflux under N_2 atmosphere, 433 K	1 mmol substrate, 1 mol% catalyst, 433 K, o-xylene, 3 bar H_2, 24 h	Hy: TON 90; TOF 3.75 h^{-1}; Dh: TON 1000; TOF 15.4 h^{-1}; Stability tested up to 5 cycles of reversible hydrogen storage.
Quinoline-1,2,3,4-tetrahydroquinoline	ISAS–Co/OPNC[96]	0.5 mmol substrate, 1.5 mol% catalyst, Ar, mesitylene,393 K, 8 h	0.5 mmol substrate, 3 mol% catalyst, 1.5 bar H_2, Toluene, 393 K, 12 h 0.5 mmol substrate, 1.5 mol% catalyst, Formic acid (H_2 source), Toluene, 393 K, 1.5 h	Dh: TON 66; TOF 8.3 h^{-1}; Hy: TON 66; TOF 44 h^{-1}; Stability tested up to 6 cycles of reversible hydrogen storage.
2-methyl piperidine/2-picoline 2,6-dimethylpiperidne/ 2,6-lutidine	Pd/C[97]	20 mmol substrate, 0.03 mmol catalyst, Ar, neat, 443 K, 94 h (Internal temperature 392 K) 10 mmol substrate, Ar, neat, 443 K, 23 h (Internal temperature 401 K)	2–7 bar of H_2 pressure, 423 K, 36 h 1.6–5 bar of H_2 pressure, 423 K, 18 h	System 1: Dh: TON 607; TOF 6.5 h^{-1}; Hy: TON 600; TOF 16.7 h^{-1}; System 1: Dh: TON 334; TOF 14.5 h^{-1} Hy: TON 334; TOF 18.5 h^{-1}; Stability tested up to 2 cycles of reversible hydrogen storage.

Table 12. continued

LOHC systems	Catalysts	Dehydrogenation conditions	Hydrogenation conditions	Comments on reactivity and stability
Substituted Quinoline and other Heteroaromatics such as Indoline, isoquinoline, quinazoline, quinoxaline, and anthracene derivatives	Co-Phen@C[98]	0.50 mmol substrate, 6 mol% catalyst, n-decane, Ar, 423 K, 36 h	0.3 mmol substrate, Toluene, 500 psi H_2, 393 K, 72 h	Dh: TON 16.7; TOF 0.46 h^{-1}; Hy: TON 5.9; TOF 0.08 h^{-1}; Stability tested up to 5 cycles of reversible hydrogen storage.
Quinoline/1,2,3,4-tetrahydroquinoline	Co nanoparticles on N-doped carbon matrix Co_x/N_yC[42]	0.1 mmol substrate, 100 mg $Co_{0.14}/N_{0.11}C$, 30 bar argon pressure, Toluene, 433 K,8 h	0.1 mmol substrate, 100 mg catalyst, 5 bar H_2 pressure, 393 K, 4 h	Dh: TON 188.6; TOF 23.5 h^{-1}; Hy: TON 188.6; TOF 47.1 h^{-1}; Stability tested up to 7 cycles of hydrogenation and 5 cycles of dehydrogenation;
1,2,3,4-tetrahydroquinoline/quinoline	Co@NCNTs-800[99]	0.5 mmol substrate, 0.5 mmol K_2CO_3, 20 mg catalyst, methanol, 13 h, O_2 balloon, 353 K	0.5 mmol substrate, 10 mg catalyst, Toluene, HCOOH, 403 K, 6 h	Dh: TON 9.23; TOF 0.71 h^{-1}; Hy: TON 18.5; TOF 111.4 h^{-1}; Stability tested up to 10 cycles of hydrogenation and 6 cycles of dehydrogenation.
Dodecahydro-N-ethylcarbazole/N-ethylcarbazole	Pd/Al_2O_3-YH_3[100]	Metal/substrate ratio 0.0025, 473 K, 0.1 MPa H_2, 4 h,	Metal/substrate ratio 0.0025, 453 K, 10 MPa H_2, 2 h	Dh: TON: 1.84; TOF 0.46 h^{-1}; Hy: TON 2; TOF 1 h^{-1}; Stability tested up to 3 cycles of reversible hydrogen storage.
1,2,3,4-tetrahydroquinoline/quinoline and other quinoline derivatives	Ru_2P[101]	0.25 mmol substrate, 20 mg catalyst, mesitylene, 418 K, 24 h	0.5 mmol substrate, 15 mg catalyst, ethanol, 5 bar H_2 pressure, 333 K, 5 h	Dh: TON 540; TOF 22.5 h^{-1}; Hy: TON 822; TOF 164.4 h^{-1}; Stability tested up to 4 cycles of reversible hydrogen storage.
1,2,3,4-tetrahydroquinoline/quinoline and other heterocycles	Pd/rGO[102]	0.1 mmol substrate, 1.5 mol% catalyst, 1,2-dichlorobenzene, N_2 atmosphere, 403 K, 9 h	0.05 mmol substrate, 1.5 mol% catalyst, 15 bar H_2 pressure, 343 K, 6 h	Dh:100% conversion and productivity of $114*10^{-6}$ (mol/g_{cat} h); Hy: TON 39.6; TOF 39.6 h^{-1} at 1 h; Stability tested up to 4 cycles of reversible hydrogen storage;
Dodecahydro-N-propylcarbazole/N-propylcarbazole	$Pd/CeO_2/Al_2O_3$[40]	Mesitylene, 463 K, 1 atm	Cyclohexane, 423 K, H_2 pressure 7.0 MPa	Pd/CeAl-20: Nearly 100% reversible hydrogen storage and release in 180 min
8H–N-methyl indole/N-methyl indole	Pd/HTN[103]	0.333 mol % catalyst, 6 mmol substrate, 443 K, 8 h	0.333 mol % catalyst, 6 mmol substrate, 423 K, 6 h	Dh: TON 84624; TOF ~176.3 min^{-1}; Hy: TON 23940; TOF ~66.5 min^{-1}; Stability tested up to 5 cycles of reversible hydrogen storage.
1,2,3,4-tetrahydroquinoline/quinoline and other N-heterocyles	Co–Pz-TPA@HAP-800[104]	0.5 mmol substrate, 8.9 mol% Co, water, 15 bar compressed air, 373 K, 24 h.	0.5 mmol substrate, 8.9 mol% Co, 10 bar hydrogen, 353 K, 24 h, water	Dh: TON 10.9; TOF 0.45 h^{-1}; Hy: TON 11.3; TOF 0.47 h^{-1}; Stability tested up to 5 cycles of reversible hydrogen storage.
1,2,3,4-tetrahydroquinoxaline/quinoxaline	P-WO_3/NF[105]	40 mL 1 M KOH with 5 mM 4H–Q; P-WO_3/NF- a anode, 300 rpm, 298 K, 15 min	40 mL 1 M KOH with 5 mM Q; P-WO_3/NF -a cathode, 300 rpm, 298 K, 2 h	Dh: 100% in 30 min; Hy: 90% in 6 h; Stability tested up to 6 cycles of hydrogenation.
1,2,3,4-tetrahydroquinoxaline/quinoxaline	Pd/NF[106]	LSV range 0.90 V and −1.80 *vs.* RHE at a scanning rate of 5 mV $s^{-1,}$ 0.5 mmol 4H–Q with 40 mL of 1 M KOH in the anode cell	LSV range 0.40 V and −0.50 *vs.* RHE at a scanning rate of 1 mV s^{-1}, 0.5 mmol Q with 40 mL of 1 M KOH in the cathode cell	Dh: 100% conversion within 30 min; Hy: 95% conversion within 120 min; Stability tested up to 8 catalytic runs.
1,2,3,4-tetrahydroquinoline/quinoline	Co–N-C[107]	20 mg catalyst, 0.1 mmol substrate, MeOH, naphthalene, 1 bar N_2, 303 K, 4 h	20 mg catalyst, 0.1 mmol substrate, MeOH, naphthalene, 2 MPa H_2, 363 K, 600 rpm, 10 h, 96.4	Dh: TON 3.28; TOF 0.82 h^{-1}; Hy: TON 4.80; TOF 0.48 h^{-1}; Stability tested up to 6 catalytic runs.
Octahydrophenazine/phenazine	Pd_2Ru@SiCN[108]	2 mmol phenazine, 0.46 mol% catalyst,463 K, Ar, flow of 4–6 ml min^{-1}, diglyme, 24 h	0.46 mol% catalyst, 388 K, 50 bar H_2 pressure, dioxane/water, 24 h	Dh: TON 217.3; TOF 9.05 h^{-1}; Hy: TON 217.3; TOF 9.05 h^{-1}; Stability tested up to 7 catalytic runs.

Table 12. continued

LOHC systems	Catalysts	Dehydrogenation conditions	Hydrogenation conditions	Comments on reactivity and stability
Quinoline and other heterocycle derivatives	Pd_1-Ni_4@MIL-100(Fe)[43]	0.1 mmol substrate, 1 mol % catalyst, H_2O, Ar, 403 K, 12 h	0.1 mmol substrate, 1 mol % catalyst, H_2O, 4 atm H_2 at 333 K for 12 h	Dh: TON 100; TOF 8.3 h^{-1}; Hy: TON 75; TOF 6.3 h^{-1}; Stability tested up to 3 catalytic runs.
1,2,3,4-tetrahydroquinaldine/Quinaldine	Ni–Si/NiO-SiO_2@SiO_2 (Cat. A) Ni-phen@SiO_2–800 (Cat. B) Ni-phen@TiO_2–800 (Cat. C)[109]	1.25 mmol substrate, 20 mol % catalyst, Ar, triglyme, 473 K, 24 h	0.5 mmol substrate, 4.5 mol %, 30 bar H_2, MeOH/H_2O (1 : 1), 393 K, 16 h	CAT A: Dh: TON 3.7; TOF 0.15 h^{-1}; Hy: TON 21.1; TOF 1.3 h^{-1}; CAT B: Dh: TON 3.2; TOF 0.13 h^{-1}; Hy: TON 22.2; TOF 1.39 h^{-1}; CAT C: Dh: TON 2.6; TOF 0.11 h^{-1}; Hy: TON 21.5; TOF 1.34 h^{-1}; Stability tested up to 3 catalytic runs.
Heterocycle derivatives	Ni–Si/NiO-SiO_2@SiO_2 (Cat. A)[109]	1.25 mmol substrate, 20 mol % catalyst, Ar, triglyme, 473 K, 24 h	0.5 mmol substrate, 20 mol %, 50 bar H_2, triglyme, 393 K, 16 h	THQ/Quinoline: Dh: TON 4.7; TOF 0.2 h^{-1}; Hy: TON 5; TOF 0.3 h^{-1}.
Perhydro-N-propylcarbazole/N-propylcarbazole	Ru–Pd/Al_2O_3[110]	1 g substrate, 0.2 g catalyst, Naphthane, 453 K, 101 kPa	2 g substrate, 0.2 g catalyst, cyclohexane, 7 MPa, 423 K, 7 h	Dh: 97.1 % yield in 4 h (5.38 wt %); Hy: Complete hydrogenation in 7 h (5.43 wt %); Stability tested up to 3 cycles of reversible hydrogen storage.
N-heterocycles, N-alkylated amines, alcohols, ketone, imines	Pd_3Au_1/CNT[111]	0.2 mmol substrate, 0.3 mol % catalyst, xylene, 413 K, 24 h	0.2 mmol substrate, 0.3 mol % catalyst, xylene, 1–5 bar H_2 pressure, 353 K, 12 h	Quinoline/1,2,3,4-tetrahydroquinoline: Dh: 96 % conversion, TON 321; TOF 26.8 h^1; Hy: 76 % conversion, TON 270; TOF 22.5 h^{-1}; Stability tested up to 5 cycles of reversible hydrogen storage.
Dodecahydro-N-ethylcarbazole- N-ethylcarbazole	Co–B/Al_2O_3-YH_{3-x}[112]	473 K, 0.1 MPa H_2 pressure, 7 h	1.0 g substrate, 453 K, 10 MPa H_2 pressure, 2 h	5 wt % metal loading, Dh: 94.8 % conversion, TON 0.91; TOF 0.13 h^{-1}; Hy: Yield 96.7 %, TON 1; TOF 0.50 h^{-1}; Stability tested up to 3 cycles of reversible hydrogen storage.
Dodecahydro-N-ethylcarbazole- N-ethylcarbazole	Pd–Rh/γ-alumina[41]	24.8 mmol substrate, 0.5 g catalyst, Ar atmosphere, 453 K, 4 h	24.8 mmol substrate, 0.5 g catalyst, 60 bar H_2 pressure, 433 K 1 h	H_2 uptake 5.46 wt % H_2 release 5.55 wt %; Dh: 99.98 % conversion; Hy: 97.3 % conversion; Stability tested up to 5 cycles of reversible hydrogen storage.
Dodecahydro-N-ethylcarbazole/N-ethylcarbazole	$LaNi_{5+x}$ ($0 < x < 1$)[113]	0.1 g $LaNi_{5.5}$, 473 K, 0.1 MPa H_2, 6 h	1.0 g NEC, 0.1 g $LaNi_{5.5}$, 453 K, 7 MPa H_2, 8 h	H_2 storage capacity 5.72 wt % and H_2 release 5.61 wt % (NMR); Stability tested up to 9 cycles of reversible hydrogen storage.
Dodecahydro-N-propylcarbazole/N-propylcarbazole	$Ru_{2.5}$-$Pd_{2.5}$/H_2[114]	1 g substrate, 0.2 g catalyst, Mesitylene, 463 K, 101.3 kPa	2 g substrate, 0.2 g catalyst, Cyclohexane, 7 MPa hydrogen, 423 K	Dh: 99.7 % conversion, 4.37 wt %; Hy: 99.6 % conversion, 5.17 wt %; Stability tested up to 5 cycles of reversible hydrogen storage.
Dodecahydro-N-ethylcarbazole/N-ethylcarbazole	Rh_1Co/γ-alumina[115]	0.5 g catalyst, Ar, 453 K, h	0.5 g catalyst, 60 bar H_2 pressure, 433 K,1 h	Dh: 100 % conversion, 4.57 wt %; Hy: 99.94 % conversion, 5.75 wt %; Stability tested up to 3 cycles of reversible hydrogen storage.
1,2,3,4-tetrahydroquinaldine/quinaldine and other quinoline derivatives	$Co_{0.15}Zn_{4.85}$-NC.[116]	0.5 mmol substrate, 3 mol % catalyst, isopropanol: H_2O (2 : 1), 10 bar argon pressure, 473 K, 20 h.	0.5 mmol substrate, 3 mol % catalyst, isopropanol: H_2O (2 : 1), 6 bar H_2 pressure, 383 K, 16 h.	Dh: > 99 % conversion with > 98 % selectivity, TON 33.3; TOF 1.65 h^{-1}; Hy: > 99 % conversion with > 98 % selectivity, TON 33.3;

Table 12. continued

LOHC systems	Catalysts	Dehydrogenation conditions	Hydrogenation conditions	Comments on reactivity and stability
				TOF 2.06 h^{-1}; Stability tested up to 3 cycles of reversible hydrogen storage.
Dodecahydro-N-ethylcarbazole/N-ethylcarbazole	PdRu/SBA-15[117]	1 g substrate, 0.15 g catalyst, 453 K, 6 h	1 g substrate, 0.3 g catalyst, cyclohexane, 373 K, H_2 pressure of 5 MPa	H_2 release 5.79 wt%, dehydrogenation efficiency 100%; H_2 storage 5.78 wt%, hydrogenation efficiency 99.8%; Stability tested up to 7 cycles of reversible hydrogen storage.
Dodecahydro-N-propylcarbazole/N-propylcarbazole	Pd_1Ni/γ-alumina[118]	24.2 mmol substrate, 0.5 g catalyst, Ar atmosphere, 453 K	24.8 mmol substrate, 0.5 g catalyst, 60 bar H_2 pressure, 433 K, 1 h	H_2 release rate 73.4 mL g^{-1} min^{-1} H_2 uptake rate 99.0 mL g^{-1} min^{-1} Dh: 99.37% conversion, H_2 release 4.63 wt%; Hy: 99.06% conversion, H_2 release 5.17 wt%; Stability tested up to 3 cycles of reversible hydrogen storage.
Ethanol/ethyl acetate	Cu–Zn–Zr–Al–O[120]	LHSV at 493 K and 0.1 MPa, LHSV = 0.4 ml $gcat^{-1}$ h^{-1}	2.4 MPa, 513 K, H_2/AcOEt = 25 mol mol^{-1}, LHSV = 1 ml $gcat^{-1}$ h^{-1}	CZZA-et: Dh: Conversion 78.9 wt%, selectivity 89.5 Wt%; Hy: Ethylacetate conversion 95.8%, selectivity 0f EtOH 98.3%.
Formic acid/CO_2	Pd/mpg-C_3N_4[121]	0.5–12 M formic acid solution, 50 mg catalyst, Stir, 298 K-328 K	CO_2 and H_2, D_2O, triethylamine (2.5 mL), 50 mg catalysts, 373 K–423 K, 24 h	Dh: 144 h^{-1} Hy: 4.74 mmol with CO_2:H_2 pressure 13: 27 bar; Stability tested up to 5 cycles of dehydrogenation.
Formic acid/CO_2	Pd/Ag-Amine MSC[122]	Molar ratio HCOOH/HCOONa: 9, pH 2.5, 348 K, N_2 atmosphere	1.0 M aqueous $NaHCO_3$ solution, pH 8.5, 2.0 MPa (H_2: CO_2 = 1:1 volume ratio) 373 K, 24 h	Dh: TOF 4960 h^{-1}; Hy: TON 859 at 24 h; Stability tested up to 3 cycles of reversible hydrogen storage.
Formic acid/CO_2	PdAg/SBA-15-amine-*x* (*x* = 1–5)[123]	0.1 g catalyst, Ar, Molar ratio HCOOH/HCOONa: 9, 348 K	0.05 g catalyst, 1 M $NaHCO_3$, 2.0 MPa CO_2, H_2, 373 K, stir 24 h	Dh: 822 h^{-1}; Hy: TON 874 after 24 h; TOF 36 h^{-1}; Stability tested up to 3 cycles of reversible hydrogen storage.
Formic acid/CO_2	PdMn@S-1[124]	Catalyst to substrate ratio fixed at 0.012, Distilled water, 333 K	40 bar CO_2/H_2 pressure, 298 K – 353 K, triethylamine/NaOH	Dh: TOF 6860 h^{-1} at 333 K; Hy: Hydrogenation rate 2151 $mol_{formate}$ mol_{Pd}^{-1} h^{-1} at 353 K; Stability tested up to 5 cycles of reversible hydrogen storage.
Formic acid/CO_2	Ir_PicaSi_SiO_2[49]	288 K – 353 K, HCOOK, 50 mM catalysts, [HCOOH] = 0.5 M, pH 3.7, 353 K,	423 K, 24 h, 50 atm (CO_2:H_2 = 1:1), Ir content 0.057 mmol, [Formate] = 0.085 M, DABCO,	Dh: TOF 11200 h^{-1}, TON 5800; Hy: TON 6983, 423 K, TOF 291 h^{-1}; Stability tested up to 4 cycles of dehydrogenation.
3-(1-hydroxyethyl)-pyridine (HEP)/3-acetylpyridin (AcP)	AcP-grafted MIL-1010(Cr)[129]	20 mg sample, Ar, 1 h, 423 K – 473 K at a heating rate of 278 K min^{-1}	20 mg sample, 373 K – 473 K, H_2 (20 mLmin^{-1})	H_2 storage up to 0.33 mmol $H_2.g^{-1}$; Stability tested up to 10 cycles of reversible hydrogen storage.

agement of large volumes and the implementation of effective heat management strategies for widespread LOHC deployment.[21] Addressing these concerns necessitates collaborative efforts across academia and industries, coupled with advancements in catalyst synthesis, characterization, and performance evaluation.

For mobile applications of LOHC technology, adequate space and weight capacity for storing the LOHC system within vehicles is critical. Furthermore, automobiles must be equipped with onboard dehydrogenation reactors to perform the reaction safely and reliably. Comprehensive assessments of the LOHC system's ecotoxicity, biodegradability, mutagenicity, and overall toxicity profile are also essential to ensure environmental safety. Addressing these issues will be vital for the successful integration of LOHCs into mobile energy applications.[12]

One notable application of LOHCs is in the direct utilization of hydrogen by automobiles. Companies like Hydrogenious and Chiyoda have begun commercializing this technology, demonstrating their viability in practical settings.[130,131] For instance, H2 MOBILITY Deutschland in collaboration with Hydrogenious, Linde and Siemens Energy in Erlangen, utilizes electrolytically produced hydrogen stored in LOHCs, which is then transported to filling stations for deployment. Recently, Biswas and colleagues proposed a novel approach to further optimize the utilization of LOHCs, particularly on board a truck.[132] Their concept involves refueling stations equipped to dispense hydrogen-rich LOHCs directly from conventional pumps. Subsequently, a catalytic reactor onboard the trucks performs the dehydrogenation process, releasing hydrogen for use in mobility applications. This approach is noted for its potential cost-effectiveness compared to current LOHC supply chains.[132]

Hydrogen supply for passenger trains like the Coradia iLint from Alstom is facilitated by the Hi ERN team in Germany through their innovative LOHC system.[134] This system with ISO-designed containers, efficiently generates hydrogen and converts it into electricity, aiming to serve non-electrified rail lines across Germany. This initiative is part of a broader global trend, with approximately 17 LOHC projects identified worldwide, 11 of which are located in Germany.[131,134] Commonly utilized LOHC combinations include dibenzyl toluene/perhydro-dibenzyltoluene and toluene/methylcyclohexane. In Germany, notable projects such as AquaVentus, HECTOR, and the Helmholtz Hydrogen Cluster, among others, are advancing LOHC technology. Internationally, initiatives like HySTOC and the Orion and Green Hydrogen @Blue Danube projects in Europe, as well as global efforts like Dii Desert Energy and the Haru Oni Project, highlight the growing interest and investment in LOHCs.[133] Japan's Chiyoda Corporation is actively involved in advancing the toluene/methylcyclohexane LOHC system through projects like SPERA Hydrogen and AHEAD, aimed at stable hydrogen storage and transport, particularly for power plant applications.[134]

Looking ahead, continued technological advancements and research breakthroughs are expected to further enhance the viability of LOHCs as alternative energy carriers. With increasing investment and recognition of their potential, LOHCs hold promise for contributing to a sustainable and resilient energy future. Interdisciplinary approaches involving materials science, catalysis, and engineering are pivotal for realizing the full potential of hybrid heterogeneous catalysts in reversible hydrogen storage systems.

Acknowledgments

J. J acknowledges UGC, India for the fellowship. B.R.J acknowledges Science & Engineering Research Board, India for financial support.

Conflict of Interests

The authors declare no conflict of interest.

Keywords: Reversible hydrogen storage · Heterogeneous catalyst · Dehydrogenation · Hydrogenation · Nanoparticles

[1] Global Energy Review: CO2 Emissions in 2021, can be found under https://www.iea.org/reports/global-energy-review-co2-emissions-in-2021-2 (Accessed July 6, 2024).
[2] A. Züttel, A. Remhof, A. Borgschulte, O. Friedrichs, *Philos. Trans. R. Soc. A* **2010**, *368*, 3329–3342.
[3] D. Teichmann, W. Arlt, P. Wasserscheid, *Int. J. Hydrogen Energy* **2012**, *37*, 18118–18132.
[4] USDRIVE, Target Explanation Document: Onboard Hydrogen Storage for Light-Duty Fuel Cell Vehicles. *US Drive* **2017**, *1* (May), 1–29.
[5] M. Niermann, S. Drünert, M. Kaltschmitt, K. Bonhoff, *Energy Environ. Sci.* **2019**, *12*, 290–307.
[6] B. L. Dietrich, K. I. Goldberg, D. M. Heinekey, T. Autrey, J. C. Linehan, *Inorg. Chem.* **2008**, *47*(19), 8583–8585.
[7] G. Principi, F. Agresti, A. Maddalena, S. Lo Russo, *Energy* **2009**, *34*, 2087–2091.
[8] D. Zhao, D. J. Timmons, D. Yuan, H. C. Zhou, *Acc. Chem. Res.* **2011**, *44*(2), 123–133.
[9] M. Hirscher, V. A. Yartys, M. Baricco, J. B. von Colbe, D. Blanchard, R. C. Bowman, D. P. Broom, C. E. Buckley, F. Chang, P. Chen, Y. W. Cho, J. C. Crivello, F. Cuevas, W. I. F. David, P. E. de Jongh, R. V. Denys, M. Dornheim, M. Felderhoff, Y. Filinchuk, G. E. Froudakis, D. M. Grant, E. M. A. Gray, B. C. Hauback, T. He, T. D. Humphries, T. R. Jensen, S. Kim, Y. Kojima, M. Latroche, H. W. Li, M. V. Lototskyy, J. W. Makepeace, K. T. Møller, L. Naheed, P. Ngene, D. Noréus, M. M. Nygård, S. ichi Orimo, M. Paskevicius, L. Pasquini, D. B. Ravnsbæk, M. Veronica Sofianos, T. J. Udovic, T. Vegge, G. S. Walker, C. J. Webb, C. Weidenthaler, C. Zlotea, *J. Alloys Compd.* **2020**, *827*, 153548.
[10] P. T. Aakko-Saksa, C. Cook, J. Kiviaho, T. Repo, *J. Power Sources* **2018**, *396*, 803–823.
[11] P. C. Rao, M. Yoon, *Energies* **2020**, *13*, 6040.
[12] D. Teichmann, W. Arlt, P. Wasserscheid, R. Freymann, *Energy Environ. Sci.* **2011**, *4*, 2767–2773.
[13] P. M. Modisha, C. N. M. Ouma, R. Garidzirai, P. Wasserscheid, D. Bessarabov, *Energy Fuels* **2019**, *33*, 2778–2796.
[14] E. Spatolisano, F. Restelli, A. Matichecchia, L. A. Pellegrini, A. R. de Angelis, S. Cattaneo, E. Roccaro, *Int. J. Hydrogen Energy* **2024**, *52*, 703–717.
[15] A. Sedminek, B. Likozar, S. Gyergyek, *ACS Omega* **2024**, *9*, 6027–6035.
[16] R. Benigni, *Chem. Rev.* **2005**, *105*(5), 1767–1800.
[17] E. J. LaVoie, G. Briggs, V. Bedenko, D. Hoffmann, *Mutat. Res. Toxicol.* **1982**, *101*(2), 141–150.
[18] M. Taube, D. W. T. Rippin, D. L. Cresswell, W. Knecht, *Int. J. Hydrogen Energy* **1983**, *8*(3), 213–225.
[19] G. P. Pez, A. R. Scott, A. C. Coopper, H. Cheng, *Hydrogen storage by Reversible Hydrogenation of pi-Conjugated Substrates*, US patent **2003**, 7, 101, 530.
[20] T. He, Q. Pei, P. Chen, *J. Energy Chem.* **2015**, *24*(5), 587–594.
[21] M. S. Salman, N. Rambhujun, C. Pratthana, K. Srivastava, K. F. Aguey-Zinsou, *Ind. Eng. Chem. Res.* **2022**, *61*, 6067–6105.
[22] E. Gianotti, M. Taillades-Jacquin, J. Rozière, D. J. Jones, *ACS Catal.* **2018**, *8*, 4660–4680.
[23] K. Sordakis, C. Tang, L. K. Vogt, H. Junge, P. J. Dyson, M. Beller, G. Laurenczy, *Chem. Rev.* **2018**, *118*, 372–433.
[24] J.-Y. Cho, H. Kim, J.-E. Oh, B. Y. Park, *Catalysts* **2021**, *11*, 1497.
[25] Y. Ding, Y. Dong, H. Zhang, Y. Zhao, M. Yang, H. Cheng, *Int. J. Hydrogen Energy* **2021**, *46*, 27026–27036.
[26] J. Wang, H. Liu, S. Fan, W. Li, Z. Li, H. Yun, X. Xu, A. Guo, Z. Wang, *Energy Fuels* **2020**, *34*, 16542–16551.
[27] L. Chen, P. Verma, K. Hou, Z. Qi, S. Zhang, Y. S. Liu, J. Guo, V. Stavila, M. D. Allendorf, L. Zheng, M. Salmeron, D. Prendergast, G. A. Somorjai, J. Su, *Nat. Commun.* **2022**, *13*(1), 1092.
[28] G. Zhou, W. Liu, Y. Zhao, X. Wang, S. Chen, A. Jia, H. Xie, *J. Ind. Eng. Chem.* **2024**, *134*, 561–573.
[29] M. R. Usman, F. M. Alotaibi, R. Aslam, *Prog. React. Kinet. Mech.* **2015**, *40*(4), 353–366.

[30] O. A. Ojelade, S. F. Zaman, *Arab. J. Sci. Eng.* **2022**, *47*, 6223–6232.
[31] L. Shi, S. Qi, J. Qu, T. Che, C. Yi, B. Yang, *Int. J. Hydrogen Energy* **2019**, *44*, 5345–5354.
[32] P. Modisha, D. Bessarabov, *Energy Fuels* **2020**, *4*, 4662–4670.
[33] L. Liu, T. Zhu, M. Xia, Y. Zhu, H. Ke, M. Yang, H. Cheng, Y. Dong, *Inorg. Chem.* **2023**, *62*, 17390–17400.
[34] K. Sisáková, N. Podrojková, R. Oriňaková, A. Oriňak, *Energy Fuels* **2021**, *35*, 7608–7623.
[35] Z. Dong, A. Mukhtar, H. Lin, *Top. Catal.* **2021**, *64*, 481–508.
[36] N. Kariya, A. Fukuoka, M. Ichikawa, *Appl. Catal. A Gen.* **2002**, *233*(1–2), 91–102.
[37] D. Sebastián, E. G. Bordejé, L. Calvillo, M. J. Lázaro, R. Moliner, *Int. J. Hydrogen Energy* **2008**, *33*, 1329–1334.
[38] G. P. Pez, A. C. Coopper, A. R. Scott, (2011) *Autothermal hydrogen storage and delivery systems*, US patent 8, 003,073, **2008**.
[39] G. P. Pez, A. R. Scott, A. C. Coopper, H. Cheng, F. C. Wilhelm, A. H. Abdourazak, 2008 *Hydrogen storage by reversible hydrogenation of pi-conjugated substrates*, US patent 7, 351,395 **2005**.
[40] C. Li, Q. Zhang, Z. Xu, L. Liu, T. Zhu, Z. Chen, Y. Dong, M. Yang, *Int. J. Hydrogen Energy* **2023**, *48*, 90–100.
[41] W. Xue, H. Liu, B. Mao, H. Liu, M. Qiu, C. Yang, X. Chen, Y. Sun, *Chem. Eng. J.* **2021**, *421*, 127781.
[42] H. Su, L. H. Sun, Z. H. Xue, P. Gao, S. N. Zhang, G. Y. Zhai, Y. M. Zhang, Y. X. Lin, X. H. Li, J. S. Chen, *Chem. Commun.* **2019**, *55*, 11394–11397.
[43] J. W. Zhang, D. D. Li, G. P. Lu, T. Deng, C. Cai, *ChemCatChem* **2018**, *10*, 4966–4972.
[44] K. H. He, F. F. Tan, C. Z. Zhou, G. J. Zhou, X. L. Yang, Y. Li, *Angew. Chemie - Int. Ed.* **2017**, *56*, 3080–3084.
[45] Á. Vivancos, M. Beller, M. Albrecht, *ACS Catal.* **2018**, *8*, 17–21.
[46] R. Xu, S. Chakraborty, H. Yuan, W. D. Jones, *ACS Catal.* **2015**, *5*, 6350–6354.
[47] M. Yang, G. Cheng, D. Xie, T. Zhu, Y. Dong, H. Ke, H. Cheng, *Int. J. Hydrogen Energy* **2018**, *43*, 8868–8876.
[48] G. A. Filonenko, R. van Putten, E. N. Schulpen, E. J. M. Hensen, E. A. Pidko, *ChemCatChem* **2014**, *6*, 1526–1530.
[49] L. Tensi, A. V. Yakimov, C. Trotta, C. Domestici, J. De Jesus Silva, S. R. Docherty, C. Zuccaccia, C. Copéret, A. Macchioni, *Inorg. Chem.* **2022**, *61*, 10575–10586.
[50] J. Kothandaraman, M. Czaun, A. Goeppert, R. Haiges, J. P. Jones, R. B. May, G. K. S. Prakash, G. A. Olah, *ChemSusChem* **2015**, *8*, 1442–1451.
[51] Q. L. Zhu, Q. Xu, *Energy Environ. Sci.* **2015**, *8*, 478–512.
[52] K. C. Tan, T. He, Y. S. Chua, P. Chen, *J. Phys. Chem. C* **2021**, *125*, 18553–18566.
[53] R. Tan, Q. Ji, Y. Ling, L. Li, *Chem. Commun.* **2024**, *60*, 8186.
[54] A. García, P. Marín, S. Ordóñez, *Int. J. Hydrogen Energy* **2024**, *52*, 1113–1123.
[55] K. Müller, J. Völkl, W. Arlt, *Energy Technol.* **2013**, *1*, 20–24.
[56] C. Chu, K. Wu, B. Luo, Q. Cao, H. Zhang, *Carbon Resour. Convers.* **2023**, *6*, 334–351.
[57] C. Mevawala, K. Brooks, M. E. Bowden, H. M. Breunig, B. L. Tran, O. Y. Gutiérrez, T. Autrey, K. Müller, *Energy Technol.* **2023**, *11*, 2200892.
[58] D. Zakgeym, J. D. Hofmann, L. A. Maurer, F. Auer, K. Müller, M. Wolf, P. Wasserscheid, *Sustainable Energy Fuels* **2023**, *7*, 1213–1222.
[59] A. A. Samarov, K. Müller, P. Wasserscheid, S. P. Verevkin, *Chem. Eng. Technol.* **2024**, *47*, 739–745.
[60] E. Clot, O. Eisenstein, R. H. Crabtree, *Chem. Commun.* **2007**, *22*, 2231–2233.
[61] M. Yang, Y. Dong, S. Fei, Q. Pan, G. Ni, C. Han, H. Ke, Q. Fang, H. Cheng, *RSC Adv.* **2013**, *3*, 24877.
[62] L. Alig, M. Fritz, S. Schneider, *Chem. Rev.* **2019**, *119*, 2681–2751.
[63] A. Mukherjee, D. Milstein, *ACS Catal.* **2018**, *8*, 11435–11469.
[64] A. N. Hellman, N. A. Torquato, M. E. Foster, C. Dun, J. E. Reynolds, C. J. Yu, A. D. Tran, M. Shivanna, G. F. H. Garcia, J. Yang, Y. Chen, J. Su, J. J. Urban, M. D. Allendorf, V. Stavila, *ACS Appl. Energy Mater.* **2023**, *6*, 7353–7362.
[65] Q. Q. Zhou, Y. Q. Zou, Y. Ben-David, D. Milstein, *Chem. - A Eur. J.* **2020**, *26*, 15487–15490.
[66] K. I. Fujita, Y. Tanaka, M. Kobayashi, R. Yamaguchi, *J. Am. Chem. Soc.* **2014**, *136*, 4829–4832.
[67] V. Zubar, J. C. Borghs, M. Rueping, *Org. Lett.* **2020**, *22*, 3974–3978.
[68] I. A. Makaryan, I. V. Sedov, *Russ. J. Appl. Chem.* **2021**, *94*, 1011–1021.
[69] M. Gupta, C. Hagen, W. C. Kaska, R. E. Cramer, C. M. Jensen, S. Barbara, *J. Am. Chem. Soc.* **1997**, *267*, 840–841.
[70] W. W. Xu, G. P. Rosini, M. Gupta, C. M. Jensen, W. C. Kaska, K. Krogh-Jespersen, A. S. Goldman, *Chem. Commun.* **1997**, *23*, 2273–2274.
[71] G. van Koten, *Pure Appl. Chem* **1989**, *61*, 1681–1694.
[72] D. Morales-Morales, R. Redón, C. Yung, C. M. Jensen, *Inorganica Chim. Acta* **2004**, *357*, 2953–2956.
[73] P. Hu, E. Fogler, Y. Diskin-Posner, M. A. Iron, D. Milstein, *Nat. Commun.* **2015**, *6*, 1–7.
[74] K. I. Fujita, T. Wada, T. Shiraishi, *Angew. Chemie - Int. Ed.* **2017**, *56*, 10886–10889.
[75] S. Chakraborty, P. E. Piszel, W. W. Brennessel, W. D. Jones, *Organometallics* **2015**, *34*, 5203–5206.
[76] J. S. Sung, K. Y. Choo, T. H. Kim, A. L. Tarasov, O. P. Tkachenko, L. M. Kustov, *Int. J. Hydrogen Energy* **2008**, *33*, 2721–2728.
[77] A. N. Kalenchuk, V. I. Bogdan, S. Dunaev, L. M. Kustov, *Chem. Eng. Technol.* **2018**, *41*, 1842–1846.
[78] A. N. Kalenchuk, N. A. Davshan, V. I. Bogdan, S. F. Dunaev, L. M. Kustov, *Russ. Chem. Bull.* **2018**, *67*, 28–32.
[79] L. M. Kustov, A. L. Tarasov, B. P. Tarasov, *Int. J. Hydrogen Energy* **2013**, *38*, 5713–5716.
[80] L. Li, X. Mu, W. Liu, Z. Mi, C. J. Li, *J. Am. Chem. Soc.* **2015**, *137*, 7576–7579.
[81] H. Jorschick, P. Preuster, S. Dürr, A. Seidel, K. Müller, A. Bösmann, P. Wasserscheid, *Energy Environ. Sci.* **2017**, *10*, 1652–1659.
[82] L. Shi, Y. Zhou, S. Qi, K. J. Smith, X. Tan, J. Yan, C. Yi, *ACS Catal.* **2020**, *10*, 10661–10671.
[83] A. Kalenchuk, V. Bogdan, S. Dunaev, L. Kustov, *Fuel* **2020**, *280*, 118625.
[84] G. Zhou, T. Li, J. Chen, L. Deng, H. Xie, *Int. J. Hydrogen Energy* **2021**, *46*, 14540–14555.
[85] L. Liu, A. Corma, *Chem. Rev.* **2023**, *123*, 4855–4933.
[86] C. Jia, W. Zhong, M. Deng, J. Jiang, *J. Chem. Phys.* **2018**, *148*, 124701.
[87] S. Beniwal, W. Chai, K. Metavarayuth, T. D. Maddumapatabandi, D. M. Shakya, G. Henkelman, D. A. Chen, *J. Phys. Chem. C* **2021**, *125*, 17671–17683.
[88] L. Liu, M. Lopez-Haro, C. W. Lopes, S. Rojas-Buzo, P. Concepcion, R. Manzorro, L. Simonelli, A. Sattler, P. Serna, J. J. Calvino, A. Corma, *Nat. Catal.* **2020**, *3*, 628–638.
[89] X. Zhang, N. He, L. Lin, Q. Zhu, G. Wang, H. Guo, *Catal. Sci. Technol.* **2020**, *10*, 1171–1181.
[90] J. Jangir, B. R. Jagirdar, *Chem. – A Eur. J.* **2024**, *30*(47), e202400980.
[91] Y. Mikami, K. Ebata, T. Mitsudome, T. Mizugaki, K. Jitsukawa, K. Kaneda, *Heterocycles* **2011**, *82*, 1371–1377.
[92] D. Ge, L. Hu, J. Wang, X. Li, F. Qi, J. Lu, X. Cao, H. Gu, *ChemCatChem* **2013**, *5*, 2183–2186.
[93] J. Li, G. Liu, X. Long, G. Gao, J. Wu, F. Li, *J. Catal.* **2017**, *355*, 53–62.
[94] C. Deraedt, R. Ye, W. T. Ralston, F. D. Toste, G. A. Somorjai, *J. Am. Chem. Soc.* **2017**, *139*, 18084–18092.
[95] S. K. Moromi, S. M. A. H. Siddiki, K. Kon, T. Toyao, K. Shimizu, *Catal. Today* **2017**, *281*, 507–511.
[96] Y. Han, Z. Wang, R. Xu, W. Zhang, W. Chen, L. Zheng, J. Zhang, J. Luo, K. Wu, Y. Zhu, C. Chen, Q. Peng, Q. Liu, P. Hu, D. Wang, Y. Li, *Angew. Chemie - Int. Ed.* **2018**, *57*, 11262–11266.
[97] Y. Xie, D. Milstein, *ACS Appl. Energy Mater.* **2019**, *2*, 4302–4308.
[98] G. Jaiswal, M. Subaramanian, M. K. Sahoo, E. Balaraman, *ChemCatChem* **2019**, *11*, 2449–2457.
[99] D. Xu, H. Zhao, Z. Dong, J. Ma, *ChemCatChem* **2019**, *11*, 5475–5486.
[100] X. Yang, Y. Wu, H. Yu, M. Sun, J. Zheng, X. Li, W. Lin, Y. Wu, *Int. J. Hydrogen Energy* **2020**, *45*, 33657–33662.
[101] F. Shao, Z. Yao, Y. Gao, Q. Zhou, Z. Bao, G. Zhuang, X. Zhong, C. Wu, Z. Wei, J. Wang, *Chinese J. Catal.* **2021**, *42*, 1185–1194.
[102] A. Mollar-Cuni, S. Martín, G. Guisado-Barrios, J. A. Mata, *Carbon* **2023**, *206*, 314–324.
[103] J. Lee, B. G. Park, K. Sung, H. Lee, J. Kim, E. Nam, J. W. Han, K. An, *ACS Catal.* **2023**, *13*, 13691–13703.
[104] Y. Hu, X. Li, M. Liu, S. Bartling, H. Lund, J. Rabeah, P. J. Dyson, M. Beller, R. V. Jagadeesh, *ChemCatChem* **2024**, *16*, e202301027.
[105] S. Wang, S. Zhang, Z. Zhang, X. Guo, Y. Tan, K. Liang, X. Wang, *Mol. Catal.* **2024**, *554*, 113842.
[106] S. Wang, S. Zhang, Z. Zhang, Y. Tan, K. Liang, X. Guo, X. Kong, *Int. J. Hydrogen Energy* **2024**, *49*, 719–728.
[107] Q. Li, Z. Sun, Y. Wei, Z. Ma, L. Wang, R. Nie, *Appl. Catal. B Environ.* **2024**, *351*, 123959.
[108] D. Forberg, T. Schwob, M. Zaheer, M. Friedrich, N. Miyajima, R. Kempe, *Nat. Commun.* **2016**, *7*, 13201.
[109] P. Ryabchuk, A. Agapova, C. Kreyenschulte, H. Lund, H. Junge, K. Junge, M. Beller, *Chem. Commun.* **2019**, *55*, 4969–4972.
[110] T. Zhu, M. Yang, X. Chen, Y. Dong, Z. Zhang, H. Cheng, *J. Catal.* **2019**, *378*, 382–391.

[111] X. Cui, Z. Huang, A. P. van Muyden, Z. Fei, T. Wang, P. J. Dyson, *Sci. Adv.* **2020**, *6*, eabb3831.
[112] Y. Wu, Y. Guo, H. Yu, X. Jiang, Y. Zhang, Y. Qi, K. Fu, L. Xie, G. Li, J. Zheng, X. Li, *CCS Chem.* **2020**, *2*, 974–984.
[113] H. Yu, X. Yang, X. Jiang, Y. Wu, S. Chen, W. Lin, Y. Wu, L. Xie, X. Li, J. Zheng, *Nano Energy* **2021**, *80*, 105476.
[114] T. Zhu, R. Wang, Z. Chen, F. Ji, Y. Dong, M. Yang, *Catal. Sci. Technol.* **2022**, *12*, 4763–4775.
[115] W. Xue, H. Liu, B. Zhao, L. Ge, S. Yang, M. Qiu, J. Li, W. Han, X. Chen, *Appl. Catal. B Environ.* **2023**, *327*, 122453.
[116] K. Naveen, T. Mahvelati-Shamsabadi, P. Sharma, S. H. Lee, S. H. Hur, W. M. Choi, T. J. Shin, J. S. Chung, *Appl. Catal. B Environ.* **2023**, *328*, 122482.
[117] Y. Wang, M. Wu, X. Bai, *Fuel* **2024**, *358*, 130284.
[118] W. Xue, B. Zhao, H. Liu, X. Chen, L. Liu, *Appl. Catal. B Environ.* **2024**, *343*, 123574.
[119] M. Melchionna, M. V. Bracamonte, A. Giuliani, L. Nasi, T. Montini, C. Tavagnacco, M. Bonchio, P. Fornasiero, M. Prato, *Energy Enviro. Sci.* **2018**, *11*, 1571.
[120] J. Ding, J. Chen, *RSC Adv.* **2015**, *5*, 82822–82833.
[121] J. H. Lee, J. Ryu, J. Y. Kim, S. W. Nam, J. H. Han, T. H. Lim, S. Gautam, K. H. Chaec, C. W. Yoon, *J. Mater. Chem. A* **2014**, *2*, 9490.
[122] S. Masuda, K. Mori, Y. Futamura, H. Yamashita, *ACS Catal.* **2018**, *8*, 2277–2285.
[123] K. Mori, S. Masuda, H. Tanaka, K. Yoshizawa, M. Che, H. Yamashita, *Chem. Commun.* **2017**, *53*, 4677–4680.
[124] Q. Sun, B. W. J. Chen, N. Wang, Q. He, A. Chang, C. M. Yang, H. Asakura, T. Tanaka, M. J. Hülsey, C. H. Wang, J. Yu, N. Yan, *Angew. Chemie - Int. Ed.* **2020**, *59*, 20183–20191.
[125] I. Göttker-Schnetmann, P. White, M. Brookhart, *J. Am. Chem. Soc.* **2004**, *126* (6), 1804–1811.
[126] S. Kundu, Y. Choliy, G. Zhuo, R. Ahuja, T. J. Emge, R. Warmuth, M. Brookhart, K. Krogh-Jespersen, A. S. Goldman, *Organometallics* **2009**, *28*(18), 5432–5444.
[127] K. Zhu, P. D. Achord, X. Zhang, K. Krogh-Jespersen, A. S. Goldman, *J. Am. Chem. Soc.* **2004**, *126*(40), 13044–13053.
[128] A. V. Polukeev, R. Wallenberg, J. Uhlig, C. P. Hulteberg, O. F. Wendt, *ChemSusChem* **2022**, *15* (8), 1–10.
[129] N. Makmeesub, C. Ritvirulh, K. Choojun, T. H. Chen, Y. Poo-arporn, D. E. Resasco, T. Sooknoi, *Ind. Eng. Chem. Res.* **2020**, *59*, 17671–17679.
[130] Press Release, Erlangen hydrogen filling station is now up and running, H2 Mobility, Berlin, can be found under https://h2.live/en/press/erlangen-hydrogen-filling-station-is-up-and-running/ (Accessed September 2024).
[131] Chiyoda Corporation, SPERA HYDROGEN can be found under https://www.chiyodacorp.com/en/service/spera-hydrogen/innovations/ (Accessed 5 July 2024).
[132] S. Biswas, K. M. Sader, W. H. Green, *Energy Fuels* **2023**, *37*, 17003–17012.
[133] HI-ERN, The Train Project, can be found under https://www.hi-ern.de/de/projekte/das-zugprojekt-mit-lohc-emissionsfrei-auf-die-schiene (Accessed 5 July, 2024).
[134] H. Li, X. Zhang, C. Zhang, Z. Ding, X. Jin, *Energies* **2024**, *17*, 1940.

Manuscript received: September 16, 2024
Revised manuscript received: October 14, 2024
Accepted manuscript online: October 17, 2024
Version of record online: ■■, ■■